Available online at www.CivileJournal.org

Civil Engineering Journal

(E-ISSN: 2476-3055; ISSN: 2676-6957)

Vol. 7, No. 12, December, 2021

Slenderness Ratio and Influencing Parameters on the NL Behaviour of RC Shear Wall

A. Atmani [1*], Z. Boudaoud [1], N. Djebbar [2]

[1] *Department of Civil Engineering, Larbi Ben M'Hidi University, Oum el Bouaghi, Algeria.*

[2] *Department of Civil Engineering, Mentouri University, Constantine 1, Algeria.*

Received 15 August 2021; Revised 13 October 2021; Accepted 06 November 2021; Published 01 December 2021

Abstract

Shear walls are very efficient structural elements to resist lateral seismic disturbance. Despite the aforementioned seismic performance, recent investigations report that they have suffered from significant structural damage after recent seismic activity, even for those complying with seismic provisions. These deficiencies in resistance and deformation capacities need to be explored. This study considers the influence of plastic length Lp, concrete compressive strength f_{c28}, longitudinal reinforcement ratio ρl, transverse reinforcement ratio ρsh, reduced axial load ν, confinement zone depth CS and focusing on the geometric slenderness λ. The parametric study has been conducted through NL pushover analysis using Peform3D software. The chosen coupled shear-flexure fiber macro model was calibrated with well-known cyclic experimental specimens. The paper points out the discrepancy between the two well-known codes EC8 and ASCE/SEI 41-13. In fact, the value of the slenderness ratio (λ) that trigger the beginning of a purely flexural behaviour recommended by EC8 ($\lambda > 2$) is very different from the value of the ASCE/SEI 41-13 ($\lambda > 3$) without accounting for the effect of the reduced axial force. Finally, it was found that RCW capacities are very sensitive to f_{c28}, ν, ρl, Lp and less sensitive to ρsh and CS. However, (λ) is the most decisive factor affecting the NL wall response. A new limit of slenderness and appropriate deformations of rotations are recommended to provide an immediate help to designers and an assistance to those involved with drafting codes.

Keywords: Macro-model; Plastic Length Lp; Slenderness Ratio λ; Confinement Zone CS.

1. Introduction

Reinforced concrete (RCW) structural walls have commonly been used as building lateral force-resisting elements in regions of moderate-to-high seismic hazard, for providing an adequate stiffness and sufficient strength to ensure an elastic seismic response and an adequate ductility to dissipate energy. Structural RCW are defined as ductile, when they have the ability to deform inelastically corresponding to their displacement ductility μΔ. Despite the aforementioned seismic characteristics, technical investigations conducted after recent earthquakes in 2003 (Algeria) [1], 2010 (Chile) and 2011(Mexico), showed that the recorded structural damage (crushing, rebar buckling, and lateral instability) in concrete shear walls exceeded the level recommended by seismic regulations, even when there was compliance to design provisions [2]. Thus, questions have been raised about current design provisions and current understanding of the determinants of NL behaviour of RCW. This paper seeks to extend the understanding of the main parameters that influence NL behaviour of RCW and advocates that a performance-based approach, where performance goals rely on limit states based on damage levels, should be taken.

* Corresponding author: eng.atmani@gmail.com

http://dx.doi.org/10.28991/cej-2021-03091777

© 2021 by the authors. Licensee C.E.J, Tehran, Iran. This article is an open access article distributed under the terms and conditions of the Creative Commons Attribution (CC-BY) license (http://creativecommons.org/licenses/by/4.0/).

Therefore, a large volume of experimental data from tests on plan RCW subjected to in plane loading and documented over the past two decades was gathered [3] and utilized as a reference in the calibrating process of the numerical model for both macro-model and finite elements. This paper focuses on the NL behaviour of the ductile RCW structures. According to the value of the aspect ratio (l_w/h_w) structural walls are classified in three main groups:

- Ductile shear walls: When a wall's aspect ratio (l_w/h_w) is greater than two, and designed to ensures that plastic hinges can form at predetermined localities called confined zones (displacement ductility $\mu_\Delta \approx 4$)
- Shear walls of limited ductility: When ductile flexural hinges cannot develop in structural walls, seismically induced shear forces assume a more important role (displacement ductility $\mu_\Delta = 1.6$).
- Walls designed for elastic response: When the Principe of strength is the main parameter in the design process and response of the structure remain elastic during the expected earthquake (displacement ductility $\mu_\Delta = 6$).

The numerical simulation has been conducted using Peform3D software**.** Two type of macro model elements of RCW are implemented in the program; Shear wall element and General wall element [4]. The shear wall element consists of vertical fibers and concrete shear layer (conventional shear) as shown in Figure 1(a). While the General Wall element is used to model axial force, bending, and shear strength (conventional shear) in addition of the diagonal compression struts that can transmit shear force and consider the contribution of reinforcing steel to the shear strength through interaction with the fiber layers. In our case, we had to choose the general wall element to simulate the interaction between the shear and flexure. The chosen coupled shear-flexure fiber macro model was calibrated with well-known cyclic experimental specimens.

The study revealed, that the lateral capacities of the concrete shear walls are sensitive to the concrete resistance (f_{c28}), the reduced normal force (ν), the longitudinal reinforcement ratio (ρ_l) and the extent of the plastic hinge (L_p); while they are less sensitive to the transverse steel ratio (ρ_{sh}) and confinement zone depth CS. The slenderness ratio (λ) was, however found, the most decisive factor affecting the seismic NL wall behaviour expressed in terms of the aspect ratio (height to length, h_w/l_w). We point out the existence of a discrepancy between the two well-known codes EC8 [5] and ASCE ASCE/SEI 41-13 [6] in the definition of the slender wall. In fact, the value of the slenderness ratio (λ) that trigger the beginning of a purely flexural behaviour recommended by EC8 ($\lambda > 2$), is very different from the value of the ASCE/SEI 41-13 ($\lambda > 3$), in addition, to being expressed as the ratio of (h_w/l_w) neglecting the reduced axial force ν effect. To understand this discrepancy, we had explored the range between the slenderness ratio (λ) values of the two well-known codes and a new limit of λ is proposed. Moreover, deformation limit state values (θ_{IO}, θ_{LS}, θ_{NC}) for a normally reinforced section are recommended, since the values given in the relevant literature treat the lightly and heavily reinforced cases. The chosen value $0.5L_w$ of plastic hinge given by the codes is also discussed

The present paper is organised into five sections. The first section introduces the existing problem and outlines the research question and main objectives of this study. The second section presents the main modelling concepts commonly used by researchers. In Section 3, four commonly used experimental models, selected from the relevant scientific literature, have been used to calibrate the adopted numerical model. The fourth section deals with the parametric study by considering the main parameters that influence the NL behaviour of RCW while proposing some control tools that can be used to help the structural designer. The last section is devoted to the general conclusions and recommendations of the study.

2. Modeling

There are two main families of models used in the numerical simulation of the inelastic response of concrete shear walls structures [7].

2.1. Microscopic Models

The models are based on the finite element method and are particularly useful when studying the local behaviour of structures. The concrete wall is discretized by a set of finite elements. The use of this type of model provides local responses which faithfully reflect the observations and results of experimental tests [8-11]. However, for highly redundant systems, the computation time becomes prohibitive (convergence problems). Their use in modelling therefore becomes a choice to be discarded.

2.2. Macroscopic Models

Compared to microscopic models, macroscopic models are relatively simple and numerically efficient with a reduced computation time. Their accuracies and areas of use vary significantly from one model to another. Their implementation and their use in calculations must be done appropriately so that the results obtained will be representative and agree with those obtained from experiments [12-15]. The main macroscopic models widely implemented in numerical simulation are summarized [7]:

- Vertical-Line-Element Model (VLEM) or (Pier model);
- Three-Vertical-Line-Element Model (TVLEM);
- Multiple-Vertical-Line-Element Model (MVLEM);
- 2-D Shear Panel Element Model (2-D SPEM);
- Equivalent Truss Model (ETM);
- Fiber-Based Model (Figure 1a);
- The multi-layer shell element.

2.3. Modeling of RCSW using a Fiber Element Macro-model

The fiber element is idealized by discretizing the cross-section into a series of fiber, where each fiber is assigned a uniaxial hysteretic or simple model, simulating flexural or combined (bending-shear is introduced by the strut effect) (Figure 2a). This discretization is based on two main numerical approaches; the first based on displacement [16, 17] and the second on force [18, 19]. The displacement approach requires a fine meshing and considerable computation time. The force-based approach, on the other hand, depends on the choice of force interpolation functions that satisfies the global equilibrium of the section, thus considerably reducing the computation time. However, the results have been found to be less accurate than obtained by the first approach [20]. It should be noted that classic fiber models could not capture the NL behaviour of walls mainly controlled by shear deformations, as a result, they had to be modified in order to include the shear effect.

2.4. Categorization of Concrete Shear Walls (ASCE /SEI41-13)

The behaviour of RCSW is defined function of the geometric slenderness value λ (height/length).

- RCSW or parts of walls are considered as slender (controlled by bending) if λ greater than 3.0.
- Reinforced concrete walls or parts of walls are considered short (governed by shear) if λ is less than 1.50 and those between 1.5 and 3.0 are influenced by both bending and shear.

2.5. Modeling Aspect

It is recognized that distributed-plasticity beam-column models with fiber sections [20-22] provide a more accurate approach to simulate NL behaviour RC walls than lumped-plasticity models under both static and dynamic loads [18], because they can capture the variation of axial force in the axial-flexural interaction. This behaviour can be expressed by shear, bending, or combined shear-bending [7]. Since classic fiber model cannot capture the NL behaviour of squat walls mainly controlled by shear. Thus Fiber models must be modified to overcome this shortcoming. To better capture the shear effect (conventional and distortional), the macro-model used for the simulation is based on the fiber-based element with consideration of the strut effect; however, the shear induced by the normal force is neglected. An ultimate deformation for vertical steel is introduced to avoid an out of plane effect. The modelling work was carried out using the Perform3D software [23].

2.6. Modeling Data

The fiber behaviour laws are introduced through a uni-axial trilinear force-deformation curve (Inelastic 1D Concrete material, Inelastic Steel material Non-Buckling). These laws reflect the behaviour of the material starting from the elastic phase, passing to the elastoplastic to plastic stage until reaching failure or total loss of strength. The RCW is discretized on two main families of steel and concrete fibers (Figure 1b), where its Behavioural law is introduced:

- Behavioural law of concrete - steel (Figure 1c);
- Energy degradation factors Concrete – Rebar (Figure 1d);
- Shear from diagonal compression (Figure 1e);
- Inelastic behaviour law of the material under the effect of shear is introduced in different ways;
- Perform3D uses two methods of modelling wall elements. The first is called "Shear Wall, inelastic section, suitable for slender walls ", and the second is called "General Wall, inelastic section, used to introduce the effect shear through the strut effect ", suitable to model squat walls. The shear effect is introduced by a force-strain curve (Figure 1f);
- Y Point: yielding point, significant beginning of the behaviour NL;
- U Point: ultimate strength point reached;

- L Point: ductility limit point, significant beginning of strength loss;
- R Point: point where the minimum residual strength is reached;
- X Point: point where the deformation becomes very large, and the analysis must stop.

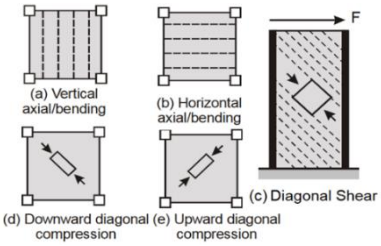

Figure 1a.Fiber-Based Mode

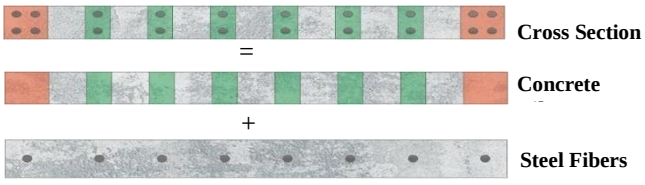

Figure 1b.discretization of concrete and steel into fiber

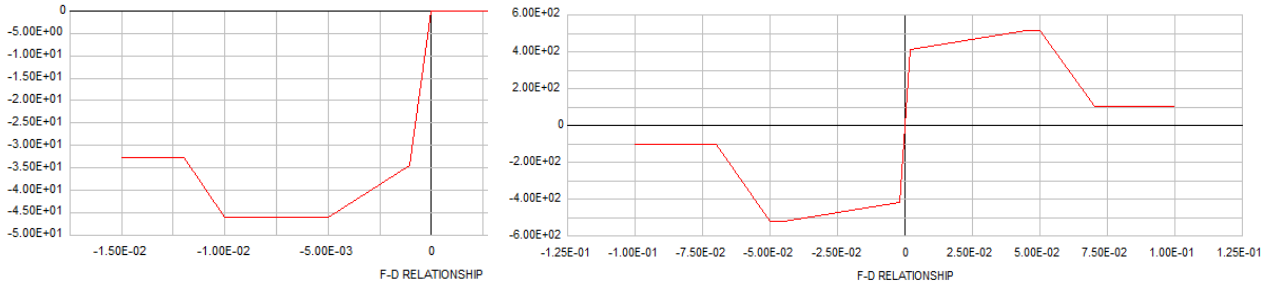

Figure 1c. Behavioural law of concrete – steel

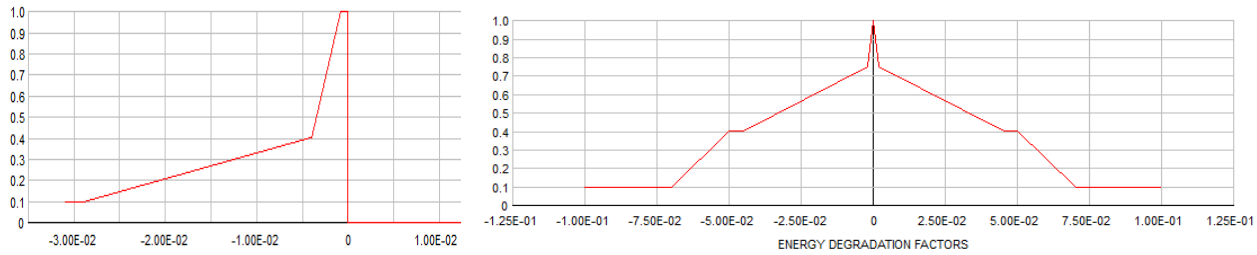

Figure 1d. Energy degradation factors Concrete – Rebar

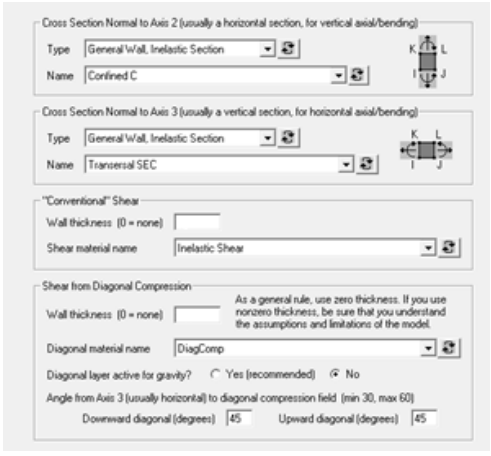

Figure 1e. Shear from diagonal compression

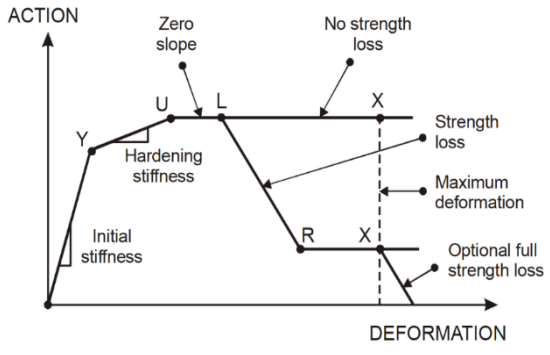

Figure 1f. Shear effect (PERFORM Action-Deformation) Relationship)

Figure 1. Modeling steps with Perfrom3D

2.7. The Degraded Loop (Trilinear Case)

- Two extreme shapes (Figure 2) may represent the trilinear degraded loop [23].
- The elastic stiffness is equal to the non-degraded value (Figure 2a), giving a minimum elastic range and a maximum strain hardening range.

- The hardening stiffness is equal to the non-degraded value (Figure 2b), resulting on a maximum elastic range and a minimum strain hardening range.
- PERFORM allows to control the elastic range, using the Unloading Stiffness Factor. A factor of 1.0 gives a maximum unloading stiffness and minimum elastic range. A factor of -1.0 gives a minimum unloading stiffness and maximum elastic range. The default is midway between these extremes [23].

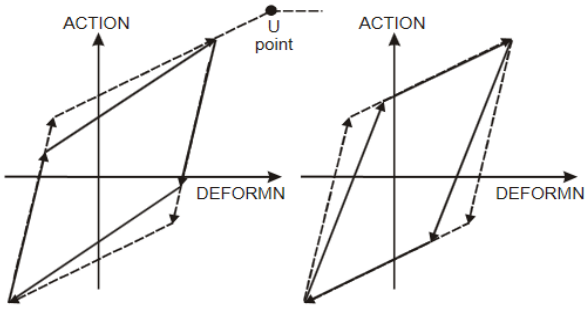

(a) Minimum Elastic Range (b) Maximum Elastic

Figure 2. Extreme Cases, Before U point

Table 1. Material cyclic energy dissipation factor [24]

Material state	Y(yield)	U(ultimate)	L(loss)	R(residual)	X(rupture)	Unloading Stiffness factor
Concrete	1	0.4	0.4	0.1	0.1	-
Steel	1	0.4	0.4	0.1	0.1	1

Shear stiffness = 0.1Gc A_{cw} [24]; Where GC = 0.4$_{EC}$ gross area

3. Model Calibration

Four experimental models (Figure 3; and Table 2) selected from the relevant scientific literature, namely SW1-1, and SW1-2 [25], RW2 [26] and PW1 [27]; the most commonly used were taken as references for the calibration of the adopted numerical analysis model. It should be noted that the limits introduced in the macro-model are those taken from the references.

Table 2. Cross sectional characteristics of sample

Designation	Dimensions (mm)	λ	f_{C28} (MPa)	L_C (mm)	υ
SW 1-1	2000x1000x125	2.0	30	200	0.214
SW 1-2	2000x1000x125	2.0	30	200	0.428
RW 2	3660x1219x102	3.0	43.64	172	0.07
PW 1	3660x3050x152	1.20	36	521	0.10

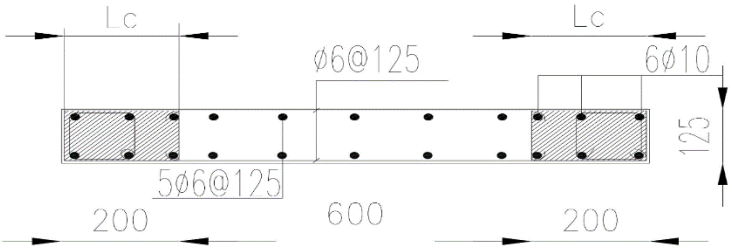

SW 1-1 and SW 1-2, Sample

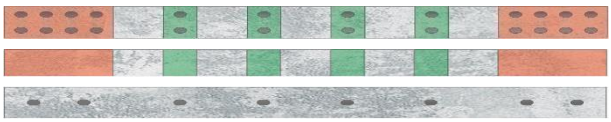

Fiber model - SW 1-1 et SW 1-2

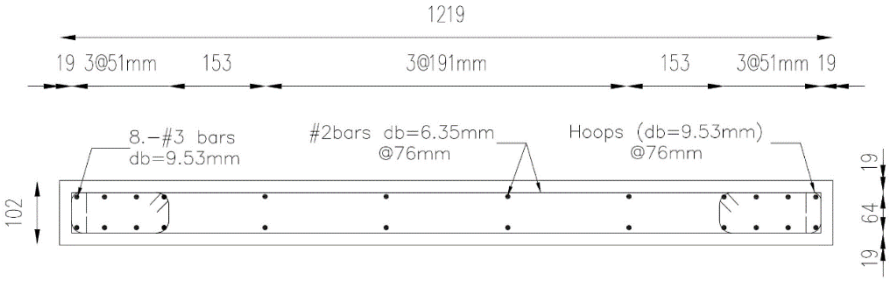

RW2, Sample

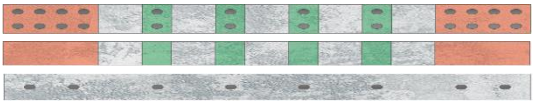

Fiber model - RW 2

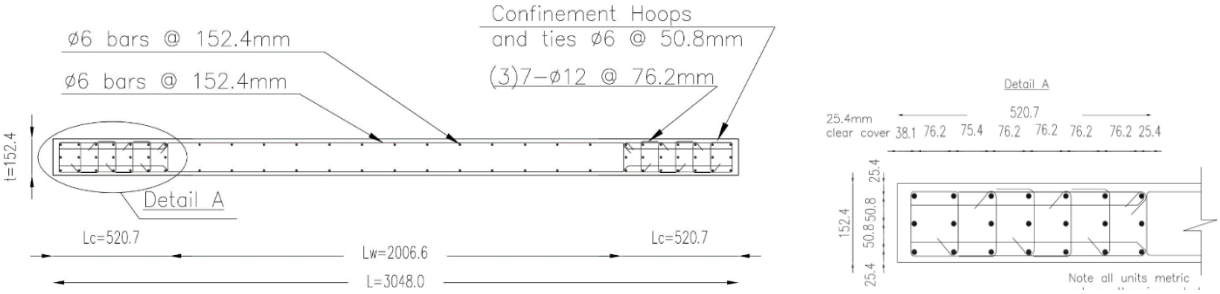

PW 1, Sample

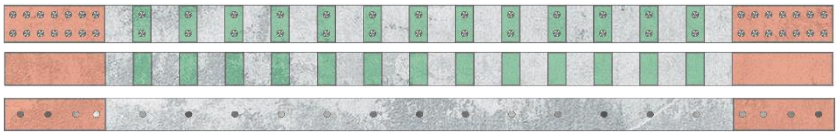

Fiber model - PW 1

Figure 3. Idealized cross section of samples

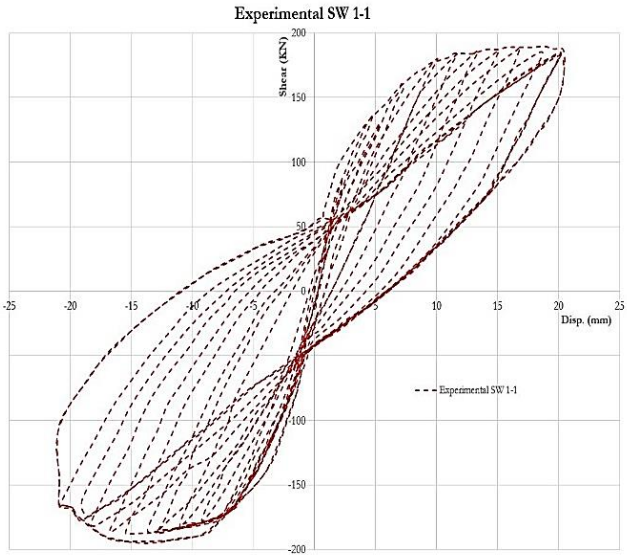

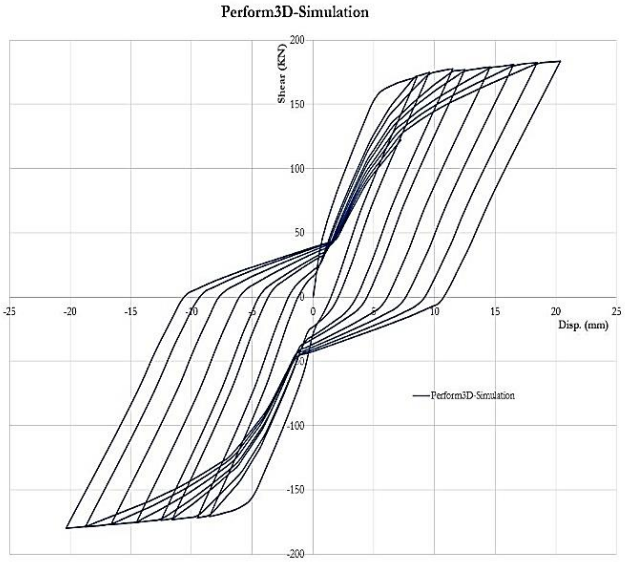

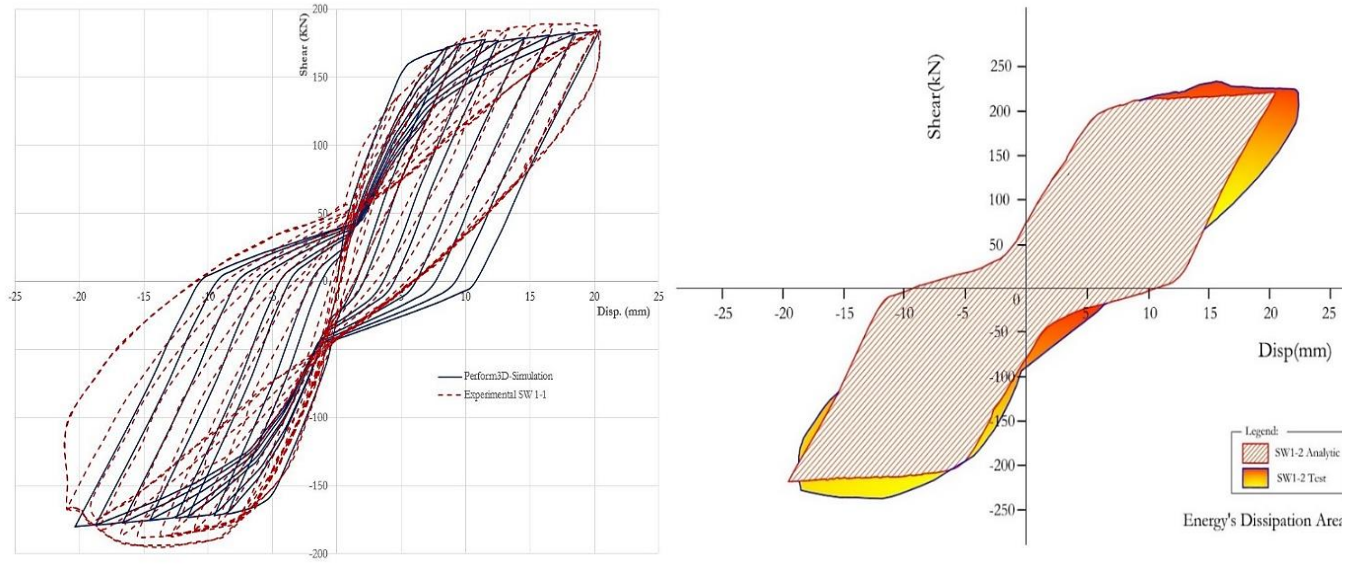

Figure 4. a) Experimental SW 1-1 vs. Perform3D-Simulation

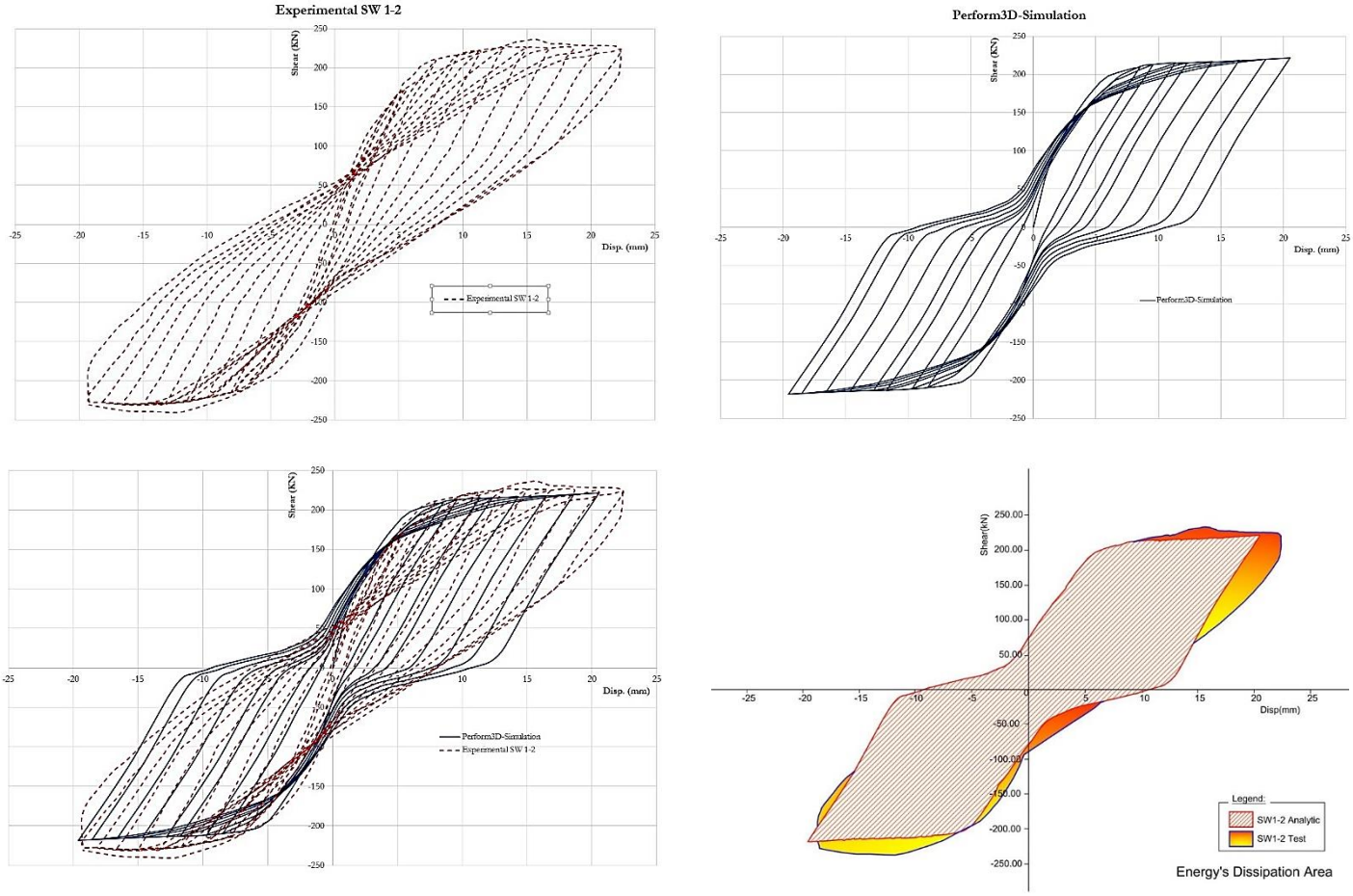

Figure 4. b) Experimental SW 1-2 vs. Perform3D-Simulation

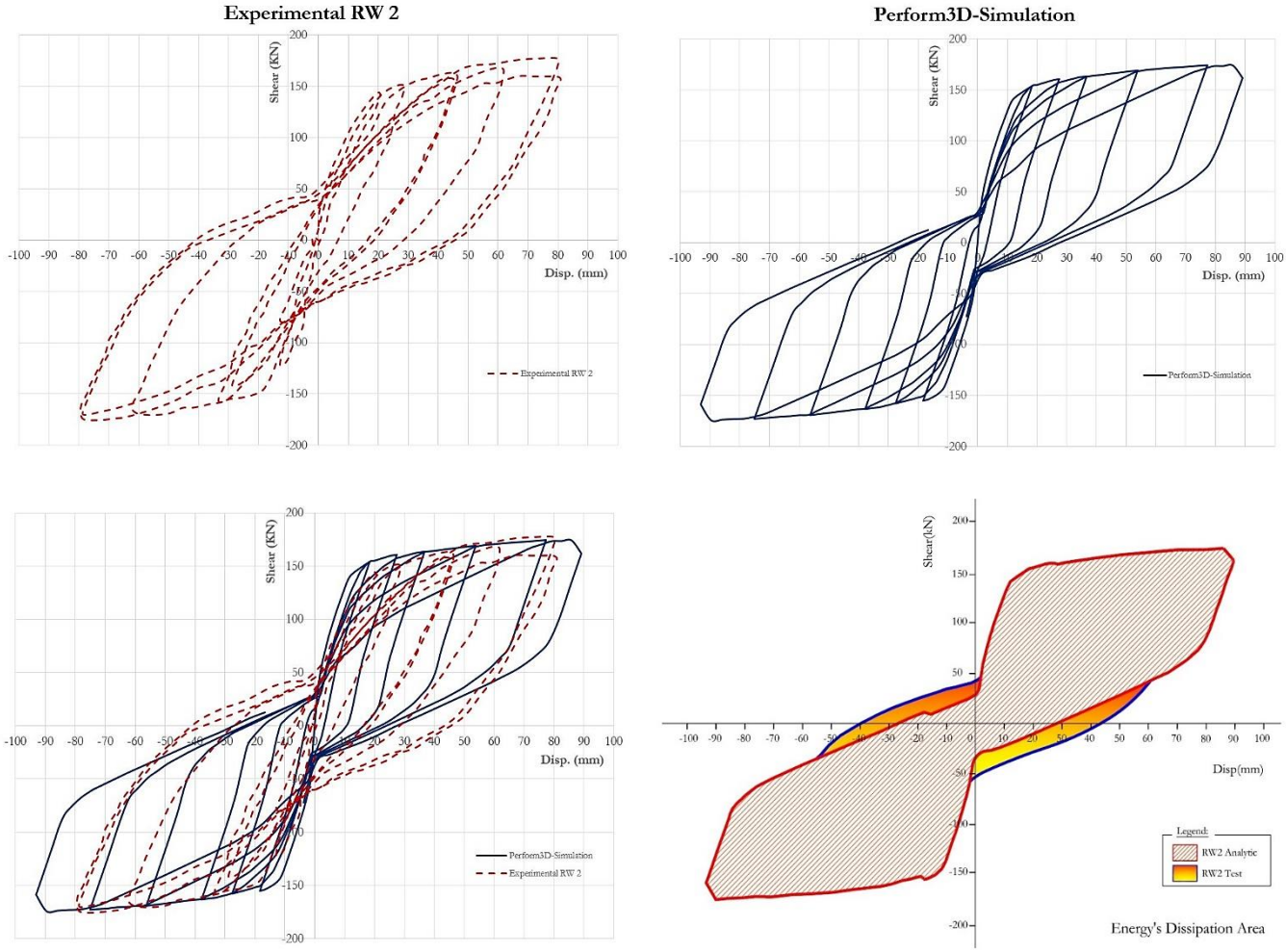

Figure 4. c) Experimental RW 2Vs Perform3D-Simulation

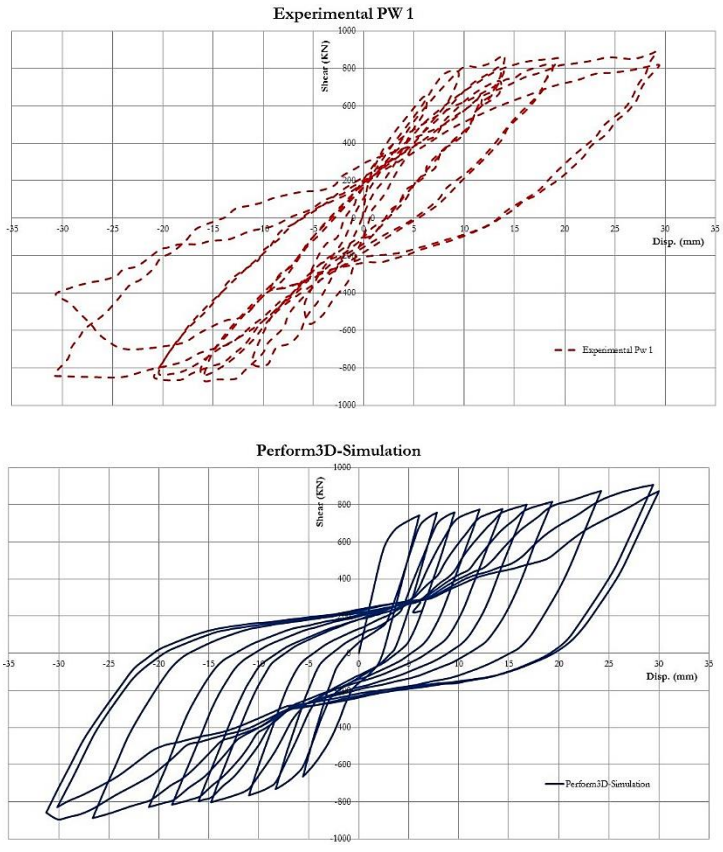

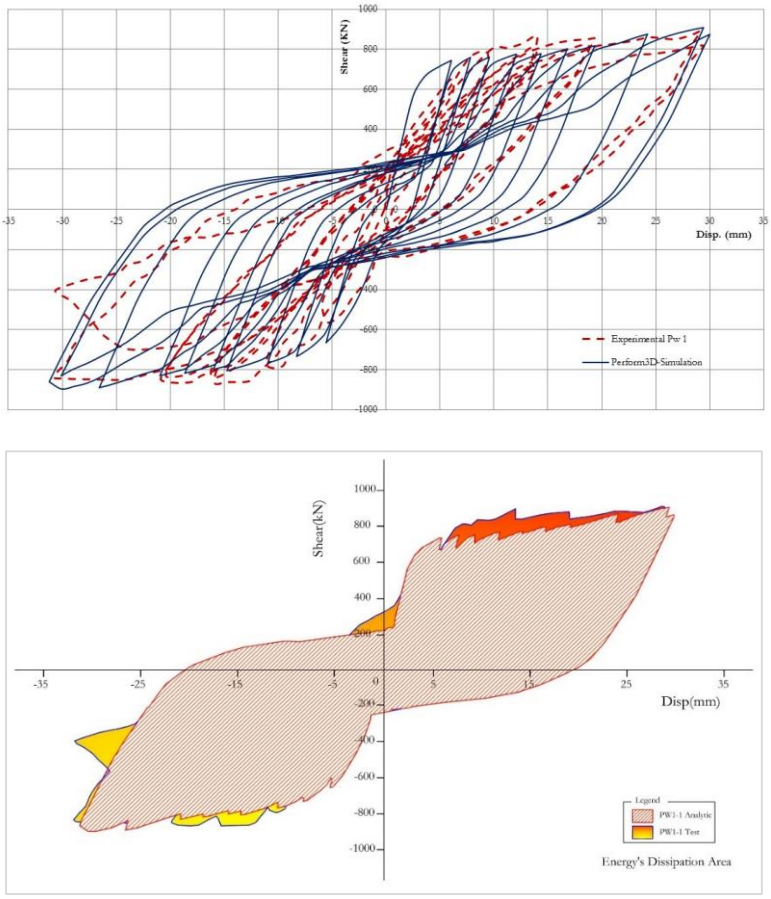

Figure 4. d) Perform3D-Simulation vs. Experimental PW 1

The theoretical curves obtained from the macro-model (Figures 4a to 4d) retrace faithfully the cyclic behaviour of the tested specimens: SW 1-1, SW 1-2, RW2, and PW1. The results presented in table 3 show that the model reliably captures the points representing the limit states in strength and in deformation of the experimental models since negligible average deviations are registered (strength 2.5 % and 0.5 % in deformation).

Table 3. Comparative results

Designation	λ	ν	V_{th} (KN)	V_{exp} (KN)	V_{th}/V_{exp}	δu^{th} (mm)	δu^{exp} (mm)	$\delta u^{th}/\delta u^{exp}$	E^{th}/E^{exp}
SW 1-1	2	0.214	183.2	187	0.98	20.37	20.35	1	0.87
SW 1-2	2	0.428	218.7	223.8	0.98	20.6	22.40	0.92	1.035
RW 2	3	0.07	174	170	0.97	55.6	54	1.03	1.23
PW1	1.2	0.10	835	858.4	0.97	55.6	54	1.03	1.097

However, if the energy is considered as a control tool, an average deviation of 12.3% is registered. In this context, Kappos [28] reports that a difference of 11% is recorded between the numerical and experimental curves. It can be concluded that the chosen macro-model, guarantees a remarkable reliability and is therefore used in the following parametric investigation.

4. Parametric Study

The study takes into consideration the parameters influencing the sectional capacity, namely:

- The concrete strength f_{c28} (20-25-30-35-40 MPa).
- The longitudinal steel ratio ρ_l (0.5, 1, and 2%); weakly, moderately and heavily reinforced.
- The transverse steel ratio ρ_{sh} (0.5, 1 and 2%), weakly, moderately and heavily confined section.
- The reduced axial stress ν (0.1, 0.20, 0.25, 0.3 and 0.35), weakly, moderate and heavily loaded section.
- The extent of the confined section Cs (0.144, 0.392, 0.5).
- The extent of the plastic hinge L_p and the geometric slenderness λ (1, 1.5, 2, 2.5, 3, and 3.5) which affect the behaviour of the structural member.

The presented results in this paper were selected from the obtained numerical ones in accordance with the requirements of the RPA99 [29] by considering the following limits:

- The concrete strength f_{c28} (25, 30 and 35 MPa), which are common values in Algeria;
- The slenderness ratio λ (2.5 and 3.5) representing the combined bending-shear and purely flexural effects;
- The reduced normal force ν (0.10 and 0.25) extreme values considered by the RPA99 [29];
- The longitudinal reinforcement ratio ρ_l (0.5%, 1% and 2%);
- The confining reinforcement ratio ρ_{sh} (lightly confined, moderately confined and highly confined);

The length of the plastic hinge was taken as Lp = 0.5Lw.

Material Limit states

The parametric study is carried out by considering the behaviour laws of the materials used, namely:

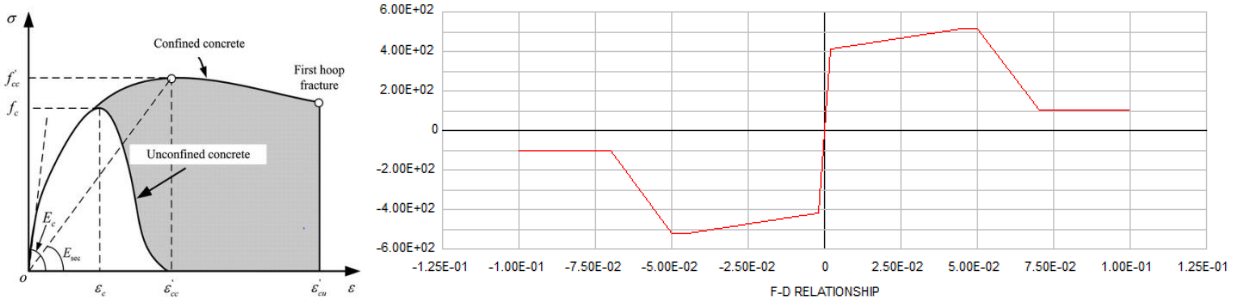

Figure 5. Confined concrete, not confined (Mander's models) and steel (trilinear)

Confined concrete: Y: (0.6fcc/Ec, 0.6fcc), U: (0.75εc, 0.6fcc), L: (1.25 εc, 0.6fcc) or:

- Y Point: first yielding point, the beginning of significate NL behaviour;
- U Point: ultimate point of strength reached;
- L Point: ductility point limit, the beginning of significate loss of strength;

Not confined concrete; Y: (0.6fc/Ec, 0.6fc,), U: (0.002, fc), L: (0.003, 0.6fc); Steel (trilinear): The ultimate deformation of the steel is taken a priori ε_{su} = 0.30 and in order to avoid the out-of-plane instability phenomenon the deformation in the strength steel is limited to:

$$\varepsilon_{sm} = \frac{\pi^2}{2}\left(\frac{t_w}{l_0}\right)^2 \xi_c + 3\varepsilon_y \quad (1)$$

t_w: thickness of the wall; l_0 : buckling length of the wall, is taken generally equal to the extent of its plastic length; [29]and limited to $0.5H_w$.

The parameter ξ_c was originally proposed by Paulay and Priestley [30] as:

$$\xi_c = 0.5\left(1+2.35\text{m}-\sqrt{5.53\text{m}^2+4.70m}\right) \quad (2)$$

Mechanical ratio of the resistance reinforcement in the confined area $\text{m} = \rho_{end}\frac{f_y}{f_c'}\rho_{end}$ can be written:

$$\rho_{end} = \frac{\rho_t - \rho_w(1-2\chi)}{2\chi} \text{ avec } \chi = \frac{l_c}{l_w} \text{ d'où } l_c = \chi l_w \quad (3)$$

4.1. Limit States for Bending Behaviour (Yielding and Ultimate)

To evaluate the ductility capacity of the elements it becomes necessary to determine the yielding and ultimate displacement. The first limit may not have a well-defined point due to the nonlinear behaviour of materials. Several definitions have been adopted by researchers in the field to evaluate the yielding displacement [31]. The yielding displacement of the equivalent elastoplastic system which has a reduced stiffness or secant stiffness is determined by reaching the first yielding of the steel or for a force $Fy = 0.75\,Fmax$. Nonlinear elastic behaviour is due to cracking of the concrete. The latter definition is considered by R. Park [31] as the most realistic one as it has been adopted in cyclic quasi-static loading tests by leading researchers in the field from different countries USA-New-Zealand-Japan-

China. Nowadays, this approach continues to be adopted [31, 32]. Therefore, it is retained for the rest of the study, i.e. the yielding displacement is assumed to be achieved if one of the two conditions is reached first:

- The yielding of the longitudinal reinforcement.
- The intersection of the line Fmax and the line through the origin and the theoretical value Fy=0.75Fmax. The ultimate limit state is assumed to be reached for whichever of the two conditions comes first ; After a 20% drop in strength, for a force Fu=0.8 Fmax or if the transverse or longitudinal steel fails or if the longitudinal steel buckles.

4.2. Limit States for Shear Behaviour (Distortion)

The residual performance within an earthquake damaged structure can be assessed through the observed damage levels, in order to take a decision about its immediate occupation, repair or its safety against collapse. In this context, Teroaka et al. [27] conducted a research work on 33 specimens of interior joints and drew a map relating the level of seismic performance with distortion and structural damage (shear angle and crack width).

γ_A: is the limiting distortion (LD) for good serviceability (0.04%); γ_B: LD for easy repair (0.4%); γ_{sl}: LD for loss of serviceability (0.5%) and γ_c: LD for difficult repair (1.0%). The schematic relationship between distortion-damage and residual seismic performance (serviceability, repair and collapse safety), assumed to vary linearly respectively. The distortion of the panels is mainly caused by the extension of the diagonal due to crack propagation and not to the compression of the concrete in the other direction. This extension can be controlled by the transverse reinforcement and the resistance reinforcement; Teroaka et al propose the following limits [33]:

- Distortion for easy repair 0.4%;
- Distortion for difficult repair 1.0%.

Using experimental data from 240 cyclic loading tests conducted on short walls, Epackachi at al. [34] recommend 0.5% distortion for yielding and 1% for limit distortion. The acceptance criteria for non-linear procedures formulated for shear-controlled elements by [32, 3] respectively are:

- IO= 0.4%; LS = 0.60% and CP = 0.75%.
- IO= 0.4%; LS = 0.75% and CP = 1.0%.

In this context and to avoid difficult repair, Graham Powell's [4] limiting distortions are adopted for the rest of the study are taken as follows:

- Du= 0.4%, Dx= 1.2%, DL= 0.75%, DR= 1.0% and no stiffness reserve is considered after yielding.

5. Influencing Parameters

5.1. Extent of the Plastic Hinge *Lp*

The plastic hinge is usually defined, as that section of the structural element, where plasticisation of concrete in compression and yielding of steel in tension zone has occurred, causing section rotation under constant ultimate effort. The shape of plastic hinges, changes from concentrated zone for linear element, to a spread area such as shear walls. It is found that plastic zone length is only slightly sensitive to boundary element reinforcement ratio, shear span ratio and axial load level (which reduces slightly the spread of plasticity along the wall); but it is significantly affected by the wall length and wall height [35]. The ultimate deformation capacity of a component depends on the ultimate curvature and plastic hinge length. Many researchers have proposed equations for the plastic hinge length L_P of RC shear walls to simulate the ultimate displacement [29, 34]. Theses equations formulated as a function of the length of the wall, the axial load υ, the moment-shear ratio M/V and the material characteristics. However, seismic code provisions recommend generally a value depending on the length of the wall (ex. Lp = $0.5L_w$).The influence of the plastic hinge length Lp, on the seismic performance of RCSW was highlighted in a previous work [36] where the combined effect of shear-flexure was considered. The numerical investigation was conducted for a variable plastic length values. The obtained results show that Lp affects the behaviour of the structure, the member and the material. The main conclusions drawn from this work are summarised as follows:

Global Behaviour

The obtained results show an appreciable gain in strength and deformation proportional to the length of the plastic hinge. This gain increases linearly until it reaches the value of Lp = 0.63 L_w (α=10) where it remains unchanged (Figure 6e). It reaches 69% in deformation and 58% in strength compared to those obtained for Lp = $0.25L_w$ (α=4). The deformation and strength value (Figure 6e) obtained while using the normative value (Lp = 0.5Lw, α=8) are up to 14% for strength and about 6% for deformation, compared to the particular value of Lp = $0.63L_w$.

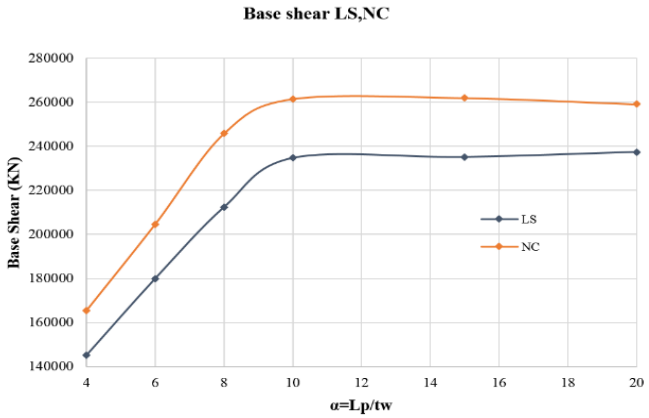

a. Base shear

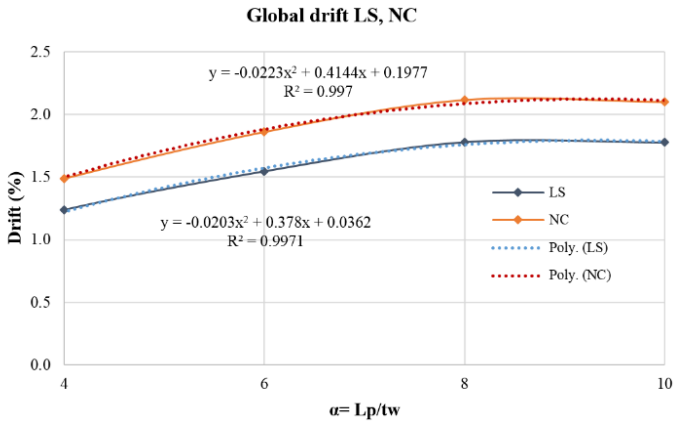

b. Global drift

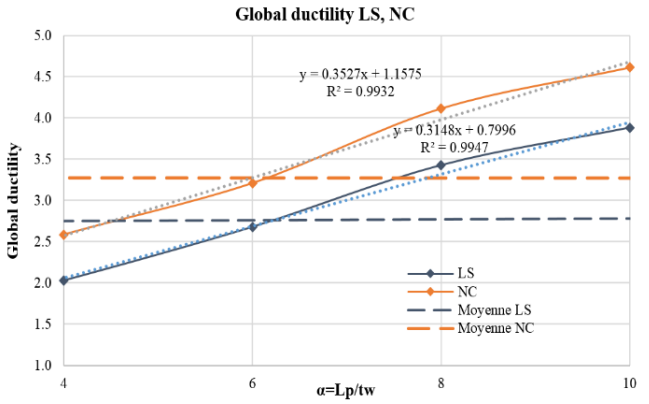

c. Ductility

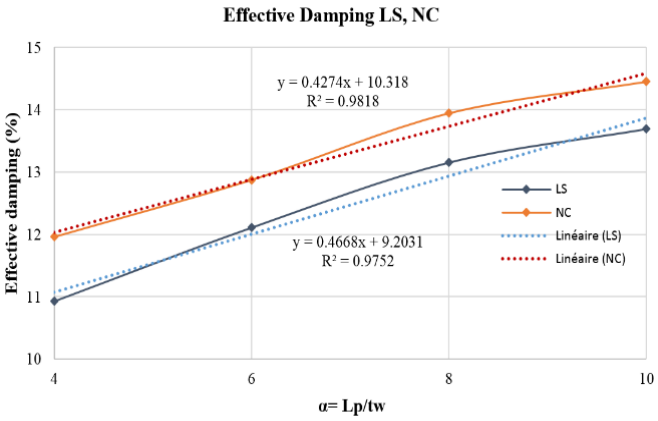

d. Effective damping

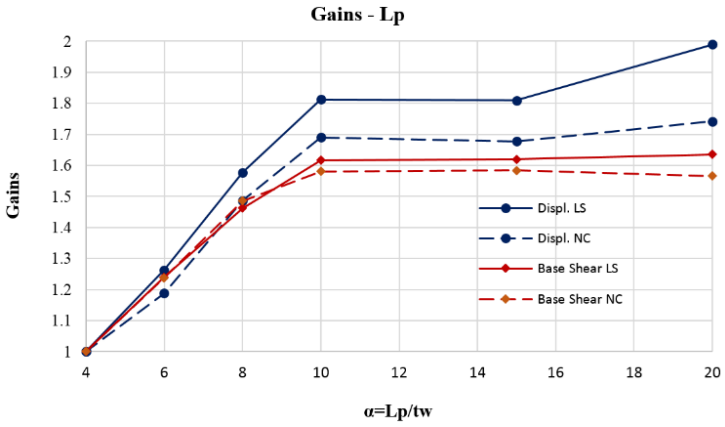

e. Capacity's gains resistance-deformation.

Figure 6. Global behaviour

The curves show that the ductility is significantly influenced by the variation of the plastic hinge length. It goes from a medium class of ductility (Figure 6e) for Lp = 0.378L_w (α=6) to a high class of ductility for Lp = 0.5L_w (Figure 6e). The recorded gain is about 18% for Lp = 0.63L_w compared to Lp = 0.25L_w.

Behaviour of the Element

The rotation of the element increases proportionally with the length of the plastic hinge Lp, until it reaches its maximum value for Lp=0.63Lw (Lp=10tw) (Figure 7a). This specific point illustrates the ultimate limit state, maximum rotation-minimum resistance. After this critical limit, the results become irrational, for the rotation decrease and the resistance increase (abnormal went back) (Figure 7b, 7c).

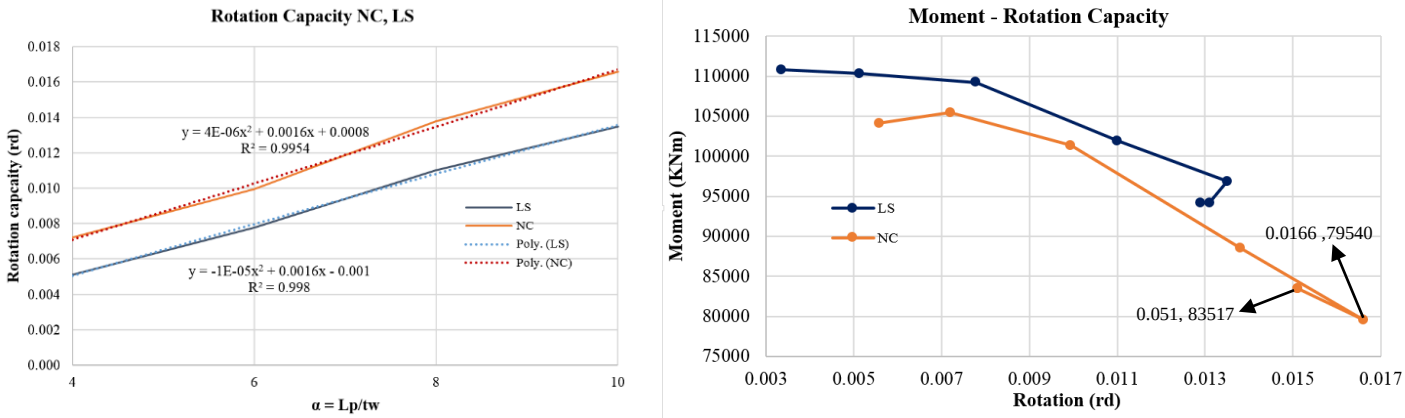

a. Rotation capacity **b. Moment capacity**

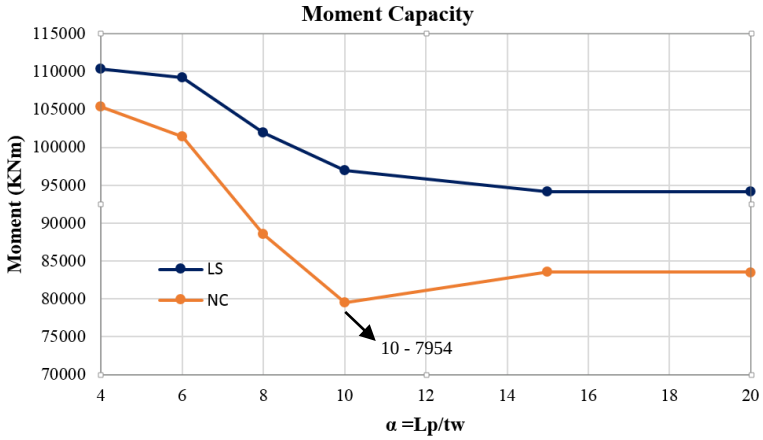

c. Moment - Rotation

Figure 7. Sectional behaviour

Effective Damping

In practical applications, the maximum inelastic displacement is the most sought-after parameter, which is directly related to ductility. The equivalent linearisation method evaluates this displacement as the maximum displacement of a linear elastic system with lower lateral stiffness and higher damping coefficient than those of the inelastic system [37]. Several analytical expressions relating effective period T_{eff}, and effective damping β_{eff} to ductility μ are nowadays evaluable within the relevant technic literature. Figure 6d shows the variation of β_{eff} function of L_P while using Iwan's relation [38], $\beta_{eff} = 0.05 + 0.0587(\mu - 1)^{0.371}$.

Table 4. Resistance and deformation results function of Lp

	Life Safety LS							Near Collapse NC						
Lp=βLw	0.189	0.252	0.378	**0.5**	**0.63**	0.645	1.26	0.189	0.252	0.378	**0.5**	**0.63**	0.645	1.26
Lp=αtw	3	4	6	**8**	**10**	15	20	3	4	6	**8**	**10**	15	20
δy(m)	0.404	0.3	0.287	0.28	0.284	0.426	0.431	0.404	0.3	0.287	0.28	0.284	0.426	0.431
Vy(KN)	83804	75663	75076	72172	73707	100668	100668	83804	75663	75076	72172	73707	100668	100668
δu(m)	0.706	0.608	0.768	0.959	1.102	1.1	1.21	0.889	0.775	0.921	1.152	1.31	1.3	1.35
Vu(KN)	138343	145196	180000	212389	234690	234104	237396	169312	165469	204708	245841	261509	261947	259115
M(KNm)	110767	110352	109236	**101967**	**96906**	94184	94145	104145	105410	101377	**88556**	**79540**	83517	83509
θ(rd)	0.00335	0.00512	0.00778	**0.0110**	**0.0135**	0.0131	0.0129	0.00558	0.00720	0.00994	**0.0138**	**0.0166**	0.0151	0.0151
μΔ LS	1.75	2.03	2.68	3.43	3.88	2.58	2.81	2.20	2.58	3.21	4.11	4.61	3.05	3.13
Drift	1.0232	0.8812	1.1130	1.3899	1.5971	1.5942	1.7536	1.2884	1.1232	1.3348	1.6696	1.8986	1.8841	1.9565
βeq	5.27	5.93	7.11	8.15	8.69	6.96	7.31	6.28	6.96	7.88	8.95	9.45	7.66	7.77
βeff	10.27	10.93	12.11	**13.15**	**13.69**	11.96	12.31	11.28	11.96	12.88	**13.95**	**14.45**	12.66	12.77

Table 5. Gain and deficiency

	Life Safety		Gain-Deficiency		Near Collapse		Gain-Deficiency	
Lp=βLw /Lp=αtw	0.5/8	0.63/10	-	**%**	0.5/8	0.63/10	-	**%**
M(KNm)	101967	96906	1.052	**-5.2**	88556	79540	1.113	**-11.3**
θ(rd)	0.0110	0.0135	0.815	**18.5**	0.0138	0.0166	0.831	**16.9**
βeff	13.15	13.69	0.961	**3.9**	13.95	14.45	0.965	**3.5**

In the same context and taking the specific point 0.63 Lw as a reference, appropriate values characterizing the limit state levels (IO, LS and NC) for bending-shear behaviour dominated by flexure and for a reduced normal force $\nu \leq 0.25$ (for an usual steel ratio) are proposed, in order to keep sufficient reserve of deformation capacity.

Table 6. Rotation limits

	ν = 0.10			**ν = 0.25**		
	θ_{IO}	**θ_{LS}**	**θ_{NC}**	**θ_{IO}**	**θ_{LS}**	**θ_{NC}**
ASCE [6]	**0.004**	0.010	0.015	0.003	0.009	0.012
FEMA [39]	**0.005**	0.010	0.015	0.003	0.006	0.009
	Under reinforced			**Over reinforced**		
G. Powel [23]	**θ_{IO}**	**θ_{LS}**	**θ_{NC}**	**θ_{IO}**	**θ_{LS}**	**θ_{NC}**
	0.005	0.010	0.015	0.003	0.006	0.009
Proposed	**Normally reinforced ν = 0.25**					
	0.0033^{rd}	0.0083^{rd}	0.0128^{rd}	-	-	-

Sectional Behaviour

The length of the plastic hinge L_p also influences the behaviour of the materials making up the section. The variation in the length of the hinge L_p causes a shift of the neutral axis of the RC shear section, leading to two families of behaviour grouped and delimited by the normative value of $0.5L_w$ (Figure 8b). This shift of the neutral axis starts from $0.57L_w$ to $0.68L_w$ leading to an optimization of the materials (compressed confined concrete) reflecting the increase of the compressed concrete area and the improvement of the cross-section rotation. This phenomenon is also recorded for concrete and steel materials if the stress state is considered as a control parameter (Figure 8a).

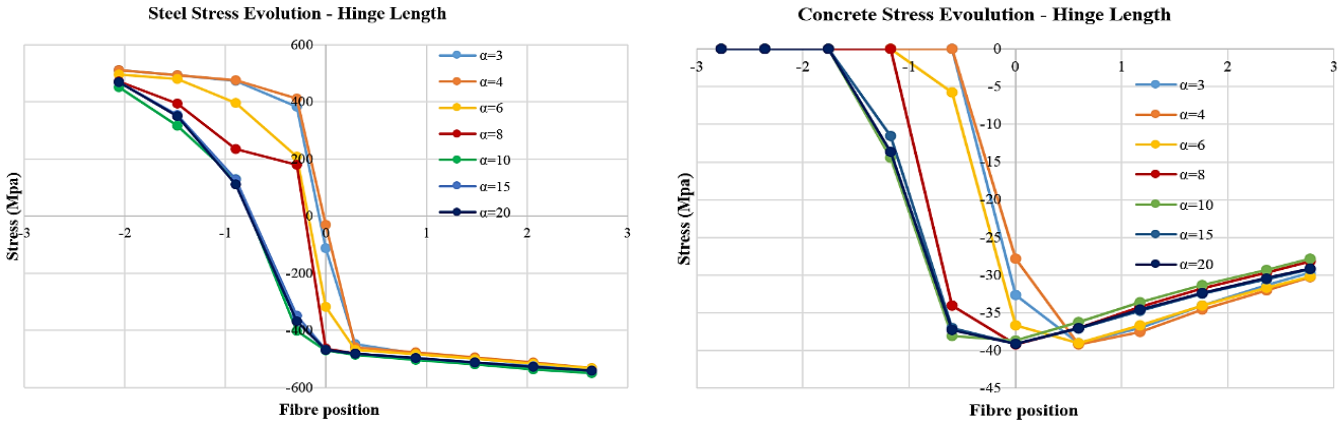

a. Steel stress evolution **b. Concrete stress evolution**

Figure 8. Sectional behaviour

The summary of the results presented shows that the code limit of $0.5L_w$ is an optimum position, for which it is adopted to conduct the rest of the study.

5.2. Concrete Strength f_{c28}

The obtained results are gathered (Figure 9) in shear-drift curves categorised according to slenderness λ and reduced force ν. It can be seen that slender walls λ = 3.5 exhibit a purely flexural behaviour. The moderately slender walls λ = 2.5 show a combined bending-shear behaviour if they are heavily loaded ν = 0.25 whatever the concrete strength. This same behaviour is observed if the walls are lightly loaded ν = 0.10, for low concrete strengths (25 MPa).

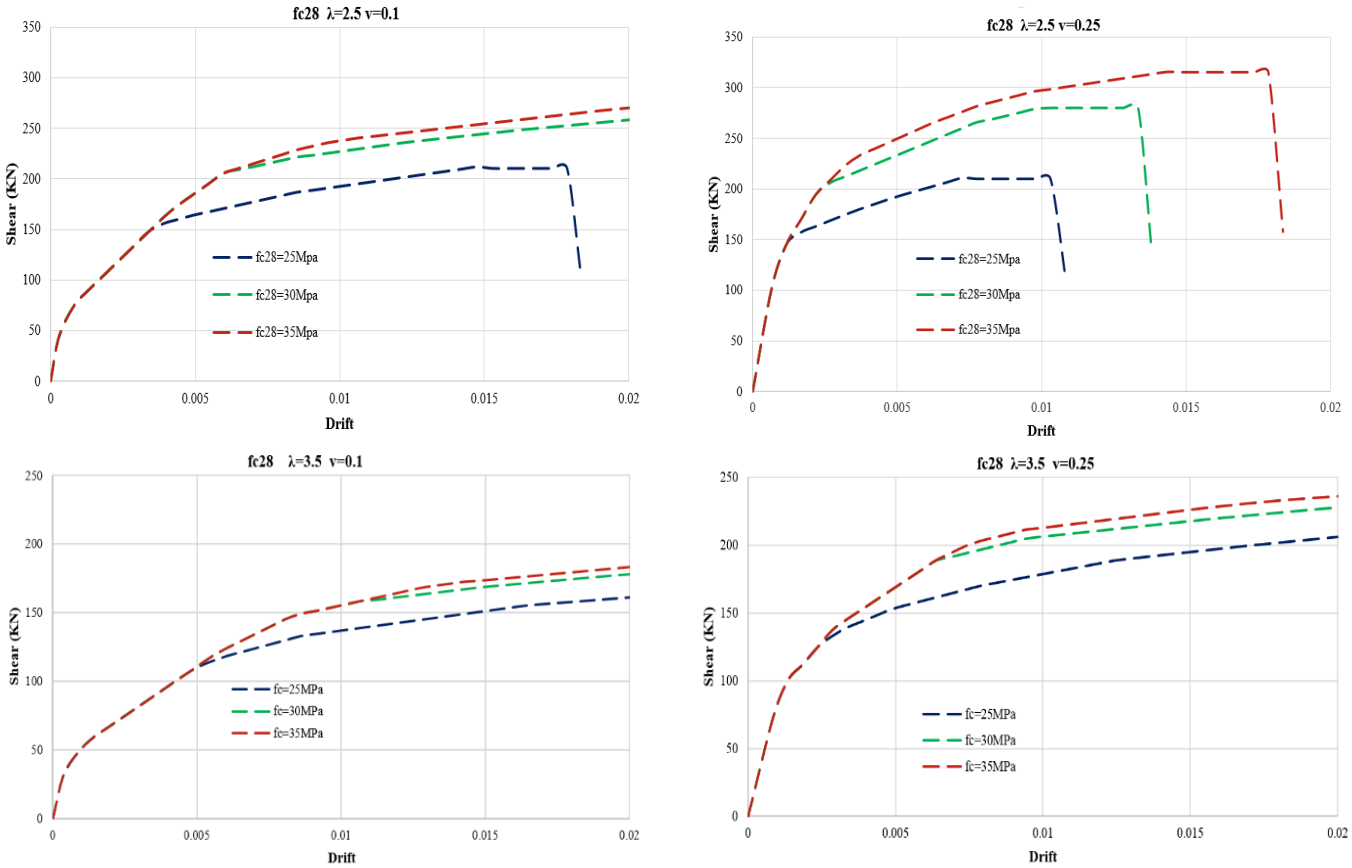

Figure 9. Influence of concrete resistance fc_{28}

Impact on the strength

- λ = 3.5 a small resistance gain (about 10%) is recorded regardless of ν.
- λ = 2.5 a small resistance gain is recorded fluctuating between 23 and 30% for ν = 0.10 and between 30 and 50% for ν = 0.25, whatever the slenderness value (Table 4)

Impact on the deformation

In terms of deformation, f_{c28} influences the yielding point recording a gain fluctuating between 6% for ν = 0.1 and ν = 0.25 if λ = 3.5. For λ = 2.5, this gain varies between 32 and 44% for f_{c28} = 30 and 35MPa if ν = 0.1, and 82% and 147% for f_{c28} = 30 and 35MPa if ν = 0.25. It should be noted that no change in this gain is recorded for a concrete strength above 30Mpa (Table 4). The concrete strength affects only the ultimate deformation of the wall having a slenderness of 2.5, where a gain of 11.7% is recorded for ν = 0.1. This gain is 29% and 72% respectively for 30 and 35 MPa of concrete strength and ν = 0.25. The same observation is made for the overall ductility where it is the shortest wall that is affected.

Impact on ductility

For λ = 2.5, the overall ductility loss recorded increases with the increase of both of the concrete strength and axial force intensity (15% and 27% if ν =0.1 respectively for f_{c28}= 30 and 35MPa and (30% if ν =0.25).

Table 4. Influence of concrete resistance fc_{28}

λ =3.5		ν =0.10		λ=3.5		ν =0.25	
Gains	**25**	**30**	**35**	**Gains**	**25**	**30**	**35**
V	161.567	178.821	184.332	V	207.009	228.612	236.733
R	1.000	1.107	1.141	R	1.000	1.104	1.144
θy	1.000	1.061	1.061	θy	1.000	1.000	1.057
θu	1.000	1.002	1.002	θu	1.000	1.000	1.000
μ_Δ	1.000	0.944	0.944	μ_Δ	1.000	1.000	0.946

λ=2.5		ν =0.10		λ=2.5		ν =0.25	
Gains	**25**	**30**	**35**	**Gains**	**25**	**30**	**35**
V	210.060	259.536	271.297	V	210.036	280.044	315.060
R	1.000	1.236	1.292	R	1.000	1.333	1.500
θy	1.000	1.317	1.439	θy	1.000	1.824	2.471
θu	1.000	1.117	1.117	θu	1.000	1.291	1.728
μ_Δ	1.000	0.848	0.776	μ_Δ	1.000	0.708	0.699

5.3. Longitudinal Steel Ratio ρ_l

The results obtained are grouped (Figure 10), in the form of families of shear-drift curves categorized according to the slenderness λ and the reduced force ν. Slender walls λ = 3.5 show a purely flexural behaviour unless the section is heavily reinforced ρ_l = 2%. Moderately slender walls λ = 2.5 show a combined flexural-shear behaviour if they are heavily loaded ν = 0.25 regardless of the reinforcement ratio ρ_l. This same behaviour is also observed if the walls are lightly loaded ν = 0.10, for reinforcement rates ρ_l =1-2% and it becomes flexural if the section is lightly reinforced (ρ_l = 0.5%).

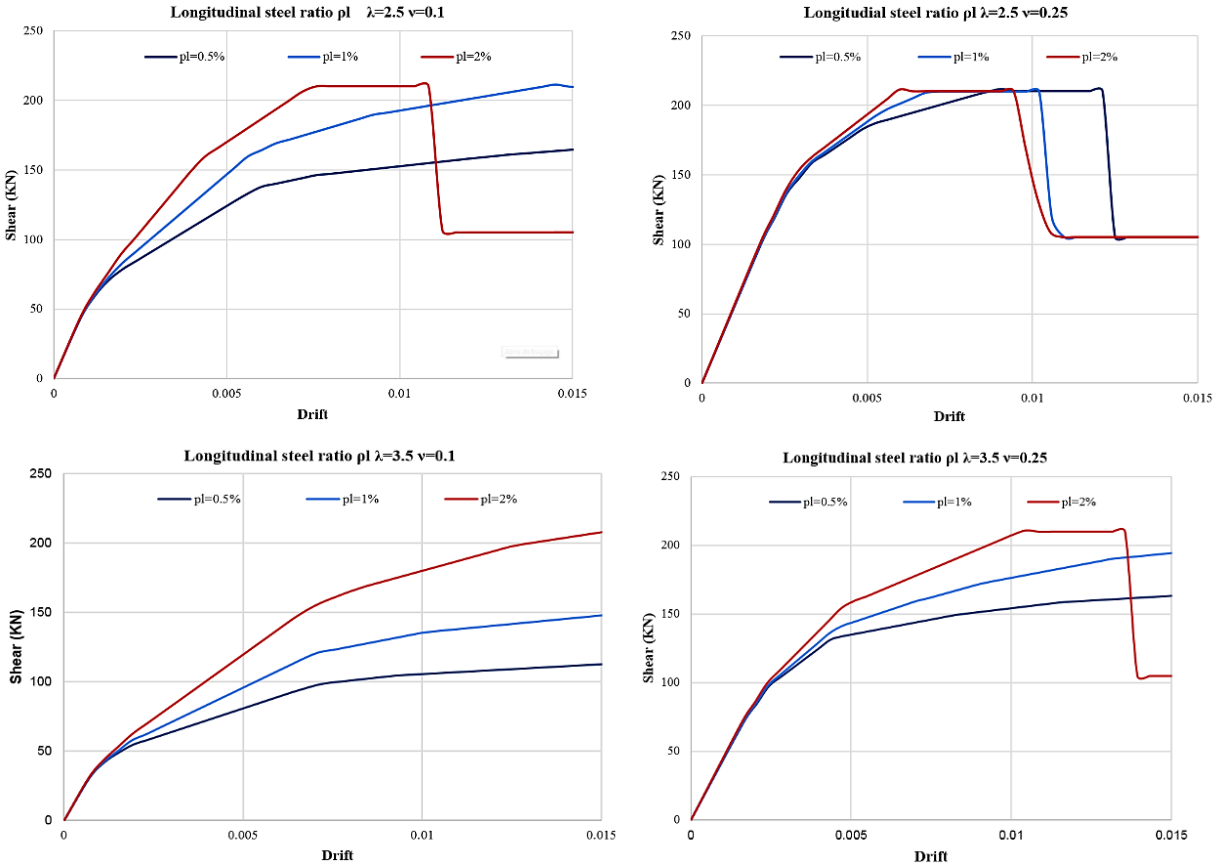

Figure 10. Influence of longitudinal steel ratio ρ_l

Table 5a. Influence of longitudinal steel ratio ρ_l

λ=3.5		ν =0.10			λ=3.5		ν =0.25	
ρ_l(%)	V	θ_y	θ_u	μ_Δ	V	θ_y	θ_u	μ_Δ
0.5	112.20	0.00430	0.0205	4.767	163.53	0.00430	0.02050	4.767
1	148.10	0.00650	0.0199	3.062	194.76	0.00510	0.02050	4.020
2	208.78	0.00600	0.01730	2.883	210.03	0.00380	0.01386	3.647
λ=2.5		**ν =0.10**			**λ=2.5**		**ν =0.25**	
ρ_l(%)	V	θ_y	θ_u	μ_Δ	V	θ_y	θ_u	μ_Δ
0.5	164.93	0.00500	0.0205	4.100	210.05	0.0030	0.01210	4.030
1	210.05	0.00390	0.01577	4.044	210.05	0.00161	0.01030	6.398
2	210.05	0.00280	0.01114	3.979	210.05	0.00161	0.00976	6.062

Table 5b. Influence of longitudinal steel ratio ρ_l (gain)

λ=3.5		ν =0.10		λ=3.5		ν =0.25	
Gains	**0.5**	**1**	**2**	**Gains**	**0.5**	**1**	**2**
V	112.20	148.10	208.78	V	163.53	194.76	210.03
R	1.000	1.247	1.630	R	1.000	1.156	1.179
θ_y	1.000	1.512	1.395	θy	1.000	1.186	0.884
θ_u	1.000	0.971	0.844	θu	1.000	0.843	0.765
μ_Δ	1.000	0.642	0.605	μ_Δ	1.000	0.843	0.765
λ=2.5		**N = 0.10**		**λ=2.5**		**ν = 0.25**	
Gains	**0.5**	**1**	**2**	**Gains**	**0.5**	**1**	**2**
V	164.93	210.05	210.05	V	210.05	210.05	210.05
R	1.000	1.273	1.273	R	1.000	1.000	1.000
θ_y	1.000	0.780	0.560	θy	1.000	0.536	0.536
θ_u	1.000	0.770	0.544	θu	1.000	0.851	0.807
μ_Δ	1.000	0.9860	0.970	μ_Δ	1.000	1.588	1.504

Impact on the Strength

A gain in resistance is registered fluctuating between 27 and 63% for ν = 0.1 and 16 and 18% for ν = 0.25 respectively for λ = 2.5 and λ = 3.5.

Impact on Deformation

Longitudinal reinforcement ratio ρ_l significantly influences the yielding point and the ultimate limit.

- For λ = 3.5 and ρ_l = 1%, an increase at the yield point up to 50% for ν = 0.1 and 19% for ν =0.25 is registered. On the case of ρ_l=2% this gain is reduced to 40% for ν = 0.1 and a loss of 12% is registered for ν =0.25.However, the ultimate limit records a deficit of deformation from 3 to 16% for ν = 0.1 respectively for ρ_l = 1 - 2%, and on the case of ν =0.25 a loss of deformation is from 16 to 25% respectively for ρ_l = 1 - 2%.
- For λ = 2.5 and ν = 0.1 a significant loss up to 22% for ρ_l = 1%, this loss is accentuated at 44% for ρ_l = 2%. For ν = 0.25 the loss of yielding deformation remains constant; 44 % (Table 5). However, the ultimate limit records a deficit from 23 to 46% for ν = 0.1 and from 15 to 19% respectively for ρ_l 1 and 2% for ν = 0.25.

Impact on Ductility

- For λ = 3.5 a registered loss of ductility (from 46% and 40%) for ν = 0.10, and form 15% to 24 % for ν = 0.25 respectively for ρl = 1% - 2%.
- For λ = 2.5 again of ductility (from 50% and 59%) for ν = 0.25, and a negligible loss is registered from 1% to 3 % respectively for ρl = 1% - 2%.

5.4. The Reduced Normal Force ν

The results obtained are gathered (Figure11), in the form of families of shear force-drift curves categorised according to slenderness λ and reduced stress ν.

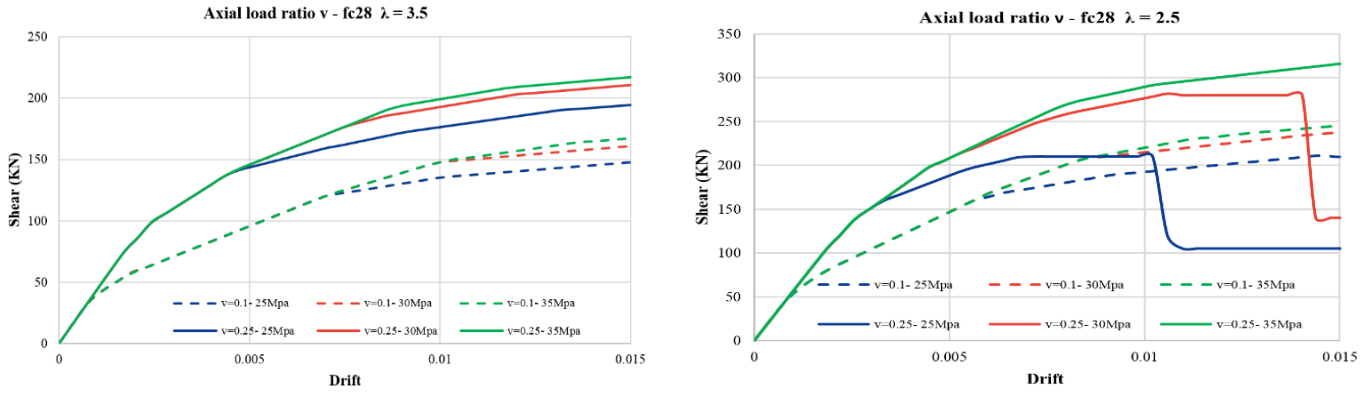

Figure 11. Influence of axial load ratio

Table 6. Influence of axial load ratio ν

λ=3.5 f_{c28} = 25MPa		λ=3.5 f_{c28} =30MPa		λ=3.5 f_{c28} = 35MPa		λ=2.5 f_{c28} = 25MPa		λ=3.5 f_{c28} =30MPa		λ=3.5 f_{c28} = 35MPa	
Gains	**ν =0.25**	**Gains**	**ν =0.25**	**Gains**	**ν =0.25**	**Gains**	**ν =0.25**	**Gains**	**ν =0.25**	**Gains**	**ν =0.25**
R	1.315	R	1.305	R	1.293	R	1.000	R	1.147	R	1.282
θ_y	0.873	θy	0.843	θy	0.829	θy	0.589	θy	0.765	θy	0.889
θ_u	0.993	θu	0.993	θu	0.993	θu	0.667	θu	0.693	θu	0.993
μ_Δ	1.138	μ_Δ	1.179	μ_Δ	1.198	μ_Δ	1.131	μ_Δ	0.906	μ_Δ	1.117

Impact on strength

For λ = 3.5 a considerable gain in resistance is registered (around 30%) when ν shifts from 0.1 to 0.25. However, this gain fluctuates between 14.7% and 28.2% respectively for f_{c28} = 30 MPa and f_{c28} = 35 MPa when ν shifts from 0.1 to 0.25 and λ = 2.5.

Impact on the deformation and ductility

The increase of ν significantly reduces the yielding rotation: 13 to 17% for λ = 3.5 and ν = 0.25 resulting in an increase in overall ductility 14 to 20%. If λ = 2.5 this reduction in yielding rotation passes from 44 and 21% respectively f_{c28} = 30 MPa and f_{c28} = 35 MPa for ν = 0.25, leading to an increase in ductility of 13 and 11.7%.

5.5. Transverse steel ratio ρ_{sh}

The results obtained are gathered (Figure 12), in the form of families of shear force-drift curves categorised according to slenderness λ and reduced stress ν.

Impact on strength

A small gain in resistance is recorded (3-8%) only for λ = 3.5.

Impact on the deformation and ductility

For λ = 2.5 ρ_{sh} has a small influence on the yielding limit (10 to 12%) if ν =0.1 and no effect for ν = 0.25. The ultimate limit is weakly affected (5 to 16%). A loss in the overall ductility is noticed (5 to 10%) for ν = 0.25. It can be concluded that the influence of the transverse reinforcement ratio is negligible.

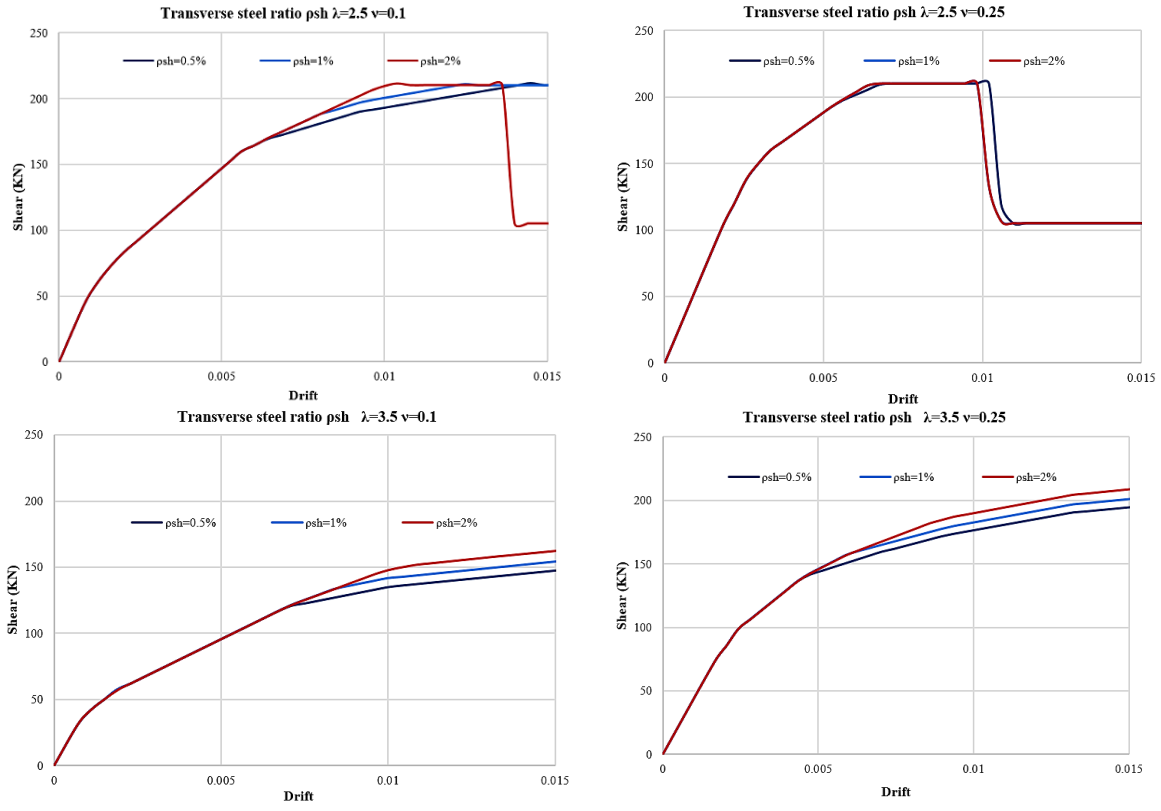

Figure 12. Influence of transversal steel ratio ρ_{sh}

5.6. Extent of the Confined Section CS

The results obtained are grouped (Figure 13), in the form of shear force-drift curves categorized according to slenderness λ and reduced axial force ν. It can be seen that the extent of the confined area has no effect on the strength and deformation capabilities of the wall regardless of its slenderness and the bearing axial force.

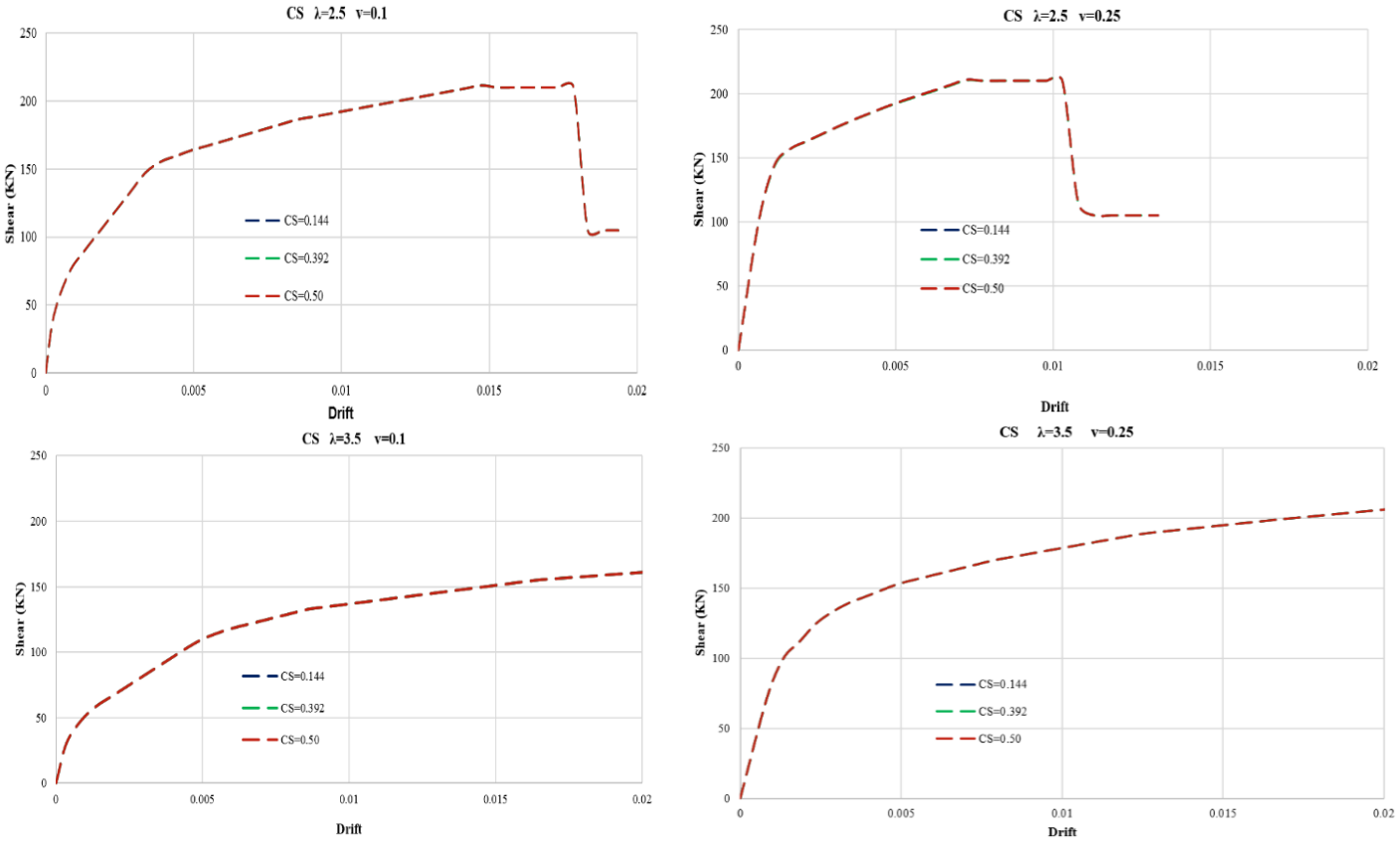

Figure 13. Influence of width of confined section CS

5.7. Slenderness Ratio λ

The increase in slenderness ratio λ enhances the element deformability and reduces its stiffness. It delays the onset of the yield point:

- 150% is recorded for λ =2.5 and 186% for λ =3.5 for ν = 0.1;
- 65% is registered for λ =2.5, and 175% if λ =3.5 for ν = 0.25.

This results in a significant loss of stiffness; hence a drop in strength of 30% for ν = 0.1 and 7% for ν =0.25. Furthermore, the ultimate deformation is also delayed in an appreciable way (sup a 90%) increasing the energy dissipation capacity. For lightly loaded RCW (ν = 0.1) flexural behaviour is noticeable for λ = 2.5, however this behaviour starts for λ = 3 for heavily loaded ones (ν = 0.25) and be dominant after λ = 3.5.

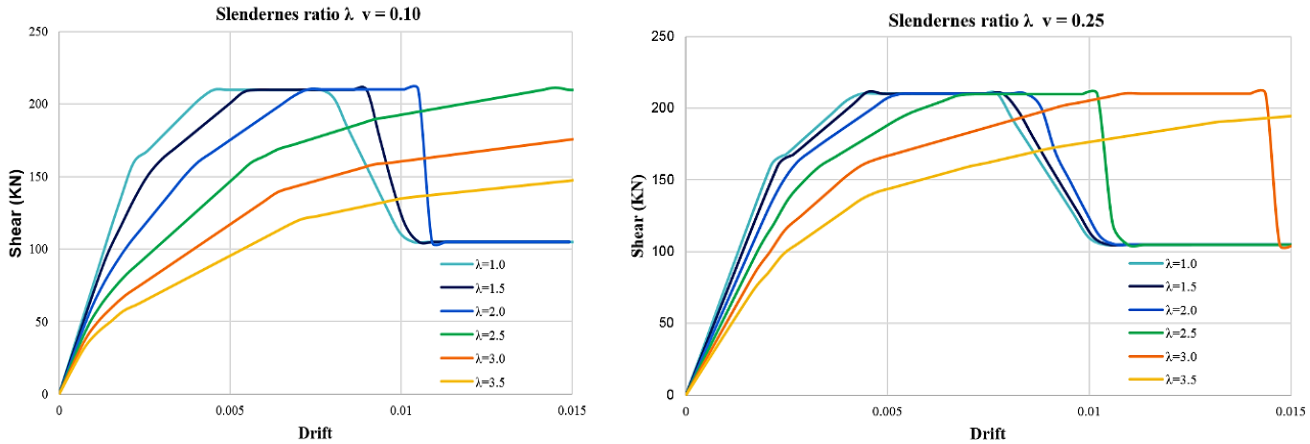

Figure 14. Influence of the slenderness ratio λ

Table 7. Influence of the slenderness ratio λ

	ν = 0.10				**ν = 0.25**			
λ	V	δy (%)	δu (%)	μ_Δ	V	δy (%)	δu (%)	μ_Δ
1	210.05	0.002	0.0076	3.45	210.05	0.002	0.0077	3.86
1.5	210.05	0.003	0.009	3.21	210.05	0.0022	0.0079	3.59
2	210.05	0.004	0.0105	2.63	210.05	0.0027	0.0084	3.11
2.5	210.05	0.006	0.0145	2.59	210.05	0.0033	0.0102	3.09
3	176.58	0.006	0.0151	2.55	210.05	0.0043	0.0147	3.42
3.5	148.1	0.006	0.0151	2.43	194.76	0.0055	0.0151	2.75

	ν = 0.10						**ν = 0.25**					
Gains	1.0	1.5	2	2.5	3	3.5	1.0	1.5	2	2.5	3	3.5
V	210.05	210.1	210.05	210.05	176.58	148.1	210.05	210.05	210.05	210.05	210.05	194.76
R	1.00	1	1	1	0.84	0.7	1.00	1	1	1	1	0.93
δy	1.00	1.27	1.82	2.54	2.72	2.86	1.00	1.1	1.35	1.65	2.15	2.75
δu	1.00	1.18	1.38	1.91	1.99	1.99	1.00	1.03	1.09	1.32	1.91	1.96
μ_Δ	1.00	0.93	0.76	0.75	0.74	0.7	1.00	0.93	0.81	0.8	0.89	0.71

5.8. Compression Strut Effect

The study of the influence of the compression strut on the behaviour of CRW was carried out using the PW1 model (already studied under cyclic effect) for a monotonic load case.it was conducted while varying the geometric slenderness (from the squat to slender wall) for two limit values of the reduced axial force $\nu = 0.1$ and $\nu = 0.25$ (from lightly to heavily loaded). This specimen was chosen because of its geometrical dimensions corresponding with commonly used RCSW (absence of the scaling effect) and the accessibility of the experimental details. Figure 15 shows that:

- The compression strut effect for RCW with slenderness $\lambda \geq 2$ is not significant (gains do not exceed 10%, Table 7);
- λ< 2 is predominantly dominated by shear effect (disturbed zone);
- λ = 2 can be considered as a demarcation point after which the flexural effect triggers although the shear effect remains important;
- λ > 2.5 the flexural effect varies increasingly (precisely for heavily loaded RCW); the flexural phenomenon starts to prevail. The element exhibits a purely flexural behaviour;
- λ = 3, for lightly loaded case ($\nu = 0.1$);
- λ = 3.5, for heavily loaded case ($\nu = 0.25$).

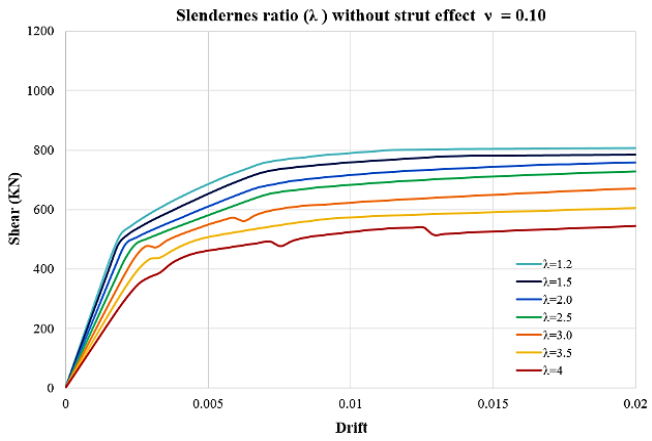

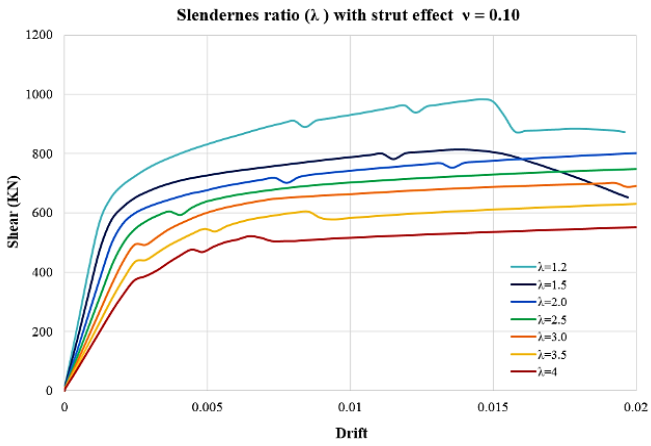

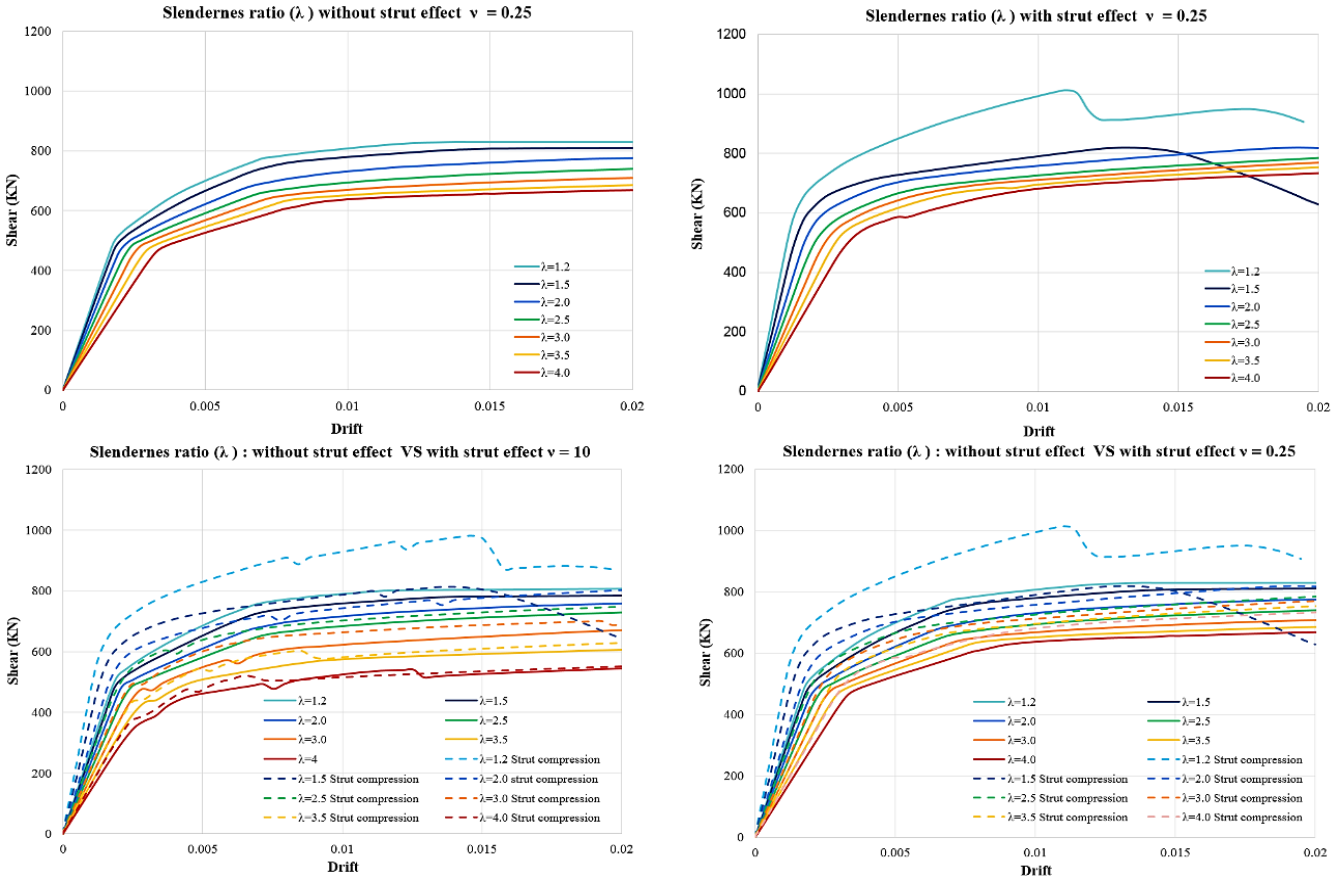

Figure 15. Influence of the compression strut on the NL response of RCW

Table 7. Influence of the compression strut on the NL response of RCW

	ν = 0.10			ν = 0.25		
λ	V	V_{strut}	Gain (%)	V	V_{strut}	Gain (%)
1.2	807.3	982.08	21.6	829	1013.62	22.3
1.5	783.3	813.11	3.8	810.5	819.65	1.1
2	758.85	802.67	5.8	776.23	819.9	5.6
2.5	728.81	748.47	2.7	739.35	785.65	6.3
3	670	700.1	4.5	709.2	770.73	8.7
3.5	605	632	4.5	686.17	754.61	10.0

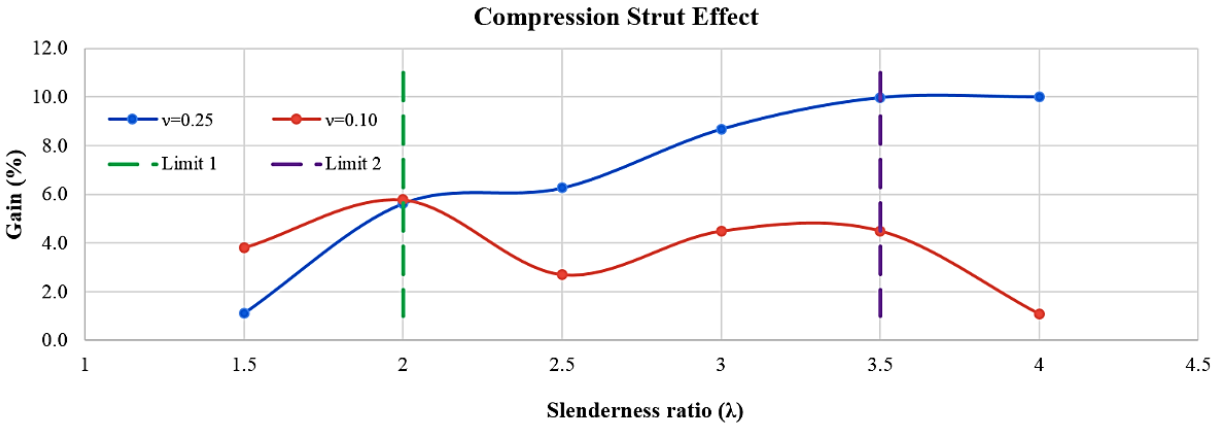

Figure 16. Registered gain due compression strut

The synthesis of the obtained results gives a clear answer on the limit slenderness beyond which the RCW will exhibit a purely flexural behaviour for both loading cases (ν=0.1 and ν=0.25). It can be concluded that the geometric slenderness of 3.5 can be considered as a threshold beyond which the RCW exhibits a purely flexural behaviour.

Contrary to EC8 and the ASCE/SEI 41-13 code which recommend a limit slenderness independently of the wall position (lightly or heavily loaded cases) and giving values of 2 and 3 respectively for a such behaviour.

6. Conclusions

6.1. Extent of the Plastic Hinge Lp

The plastic length significantly affects the strength and deformation of wall structures for values $0.25Lw \leq L_p \leq 0.63Lw$. The strength and deformation gain increases linearly until reaching $L_P = 0.63lw$ where it remains unchanged. This specific value characterises the ultimate limit state beyond which the obtained results become irrational. The normative value of $L_P = 0.5Lw$ limits the incursion into the plastic domain providing an additional safety margin (20% in deformation). The variation of the plastic length causes a shift of the neutral axis of the web section forming two behaviour families ($\sigma - \varepsilon$) delimited by the normative value of 0.5Lw. This shift is more pronounced between 0.57Lw and 0.63Lw leading to an optimisation of materials (confined concrete in compression) resulting in a larger confined area increasing thus the rotation capacity. Rotation values consistent with Limit state deformations (I.O), (L.S), (N.C) for bending-shear behaviour are proposed for a conventional steel reinforcement: $\theta_{IO} = 0.0033^{rd}$, $\theta_{LS} = 0.0083^{rd}$, $\theta_{NC} = 0.0128^{rd}$.

6.2. Concrete Strength f_{c28}

The increase of fc_{28} improves the strength (up to 50% gain) of the heavily loaded slender walls (λ=2.5) and decreases the ductility (30% of loss is recorded). However, it has no significant effect for slender walls (λ=3.5).

6.3. Longitudinal Reinforcement Ratio ρl

The increase in ρ_l leads to a significant gain in strength (up to a 50% gain) for lightly loaded slender walls (v=0.1 for λ = 2.5-3.5). Whereas a loss in ductility is noticed (25 and 40%) respectively for v = 0.25 and v=0.1 for (λ = 2.5 - 3.5). The ultimate steel deformation ε_{su}=0.30 is recommended in order to avoid the out-of-plane instability phenomenon.

6.4. The Reduced Axial Force ν

Reduced axial force ν improves slightly the strength of slender walls only for (λ=3.5). However, it reduces the yielding strength leading to a substantial increase in ductility for λ = 2.5.

6.5. Transverse Reinforcement Ratio ρ_{sh}

For λ = 3.5 ρ_{sh} has a small effect on the capacity of resistance for ν =0.1 and 0.25; for λ = 2.5 ρ_{sh} has a small effect on the capacity of resistance if ν = 0.1 and no effect if ν = 0.25; the transverse reinforcement ratio ρ_{sh} has a low effect on the deformation capacity. In order to achieve a rational confinement ratio, an effective limit of the transverse reinforcement ratio (ρ_{sh} =1%) is recommended.

6.6. Extent of the Confined Section CS

The extent of the confined area has no effect on the strength and deformation capabilities of the web (regardless of its slenderness and its bearing axial force).

6.7. Compression Strut and Slenderness Ratio λ Effect

The effect of the compression strut for RCW with slenderness $\lambda \geq 2$ is negligible (gains do not exceed 10%), however, it will be significant for squat RCW where these gains can exceed 20%. The increase in slenderness ratio λ, favours the deformability of the wall, reducing its stiffness. It delays the onset of the yield point (ranging from 65% to 186%) which leading to a consequent loss of stiffness resulting in a drop in strength. The ultimate deformation is significantly delayed (over 90%) thus increasing the energy dissipation capacity.

It should be pointed out that for lightly loaded shear walls (ν = 0.1) the flexural behaviour is noticeable for a slenderness ratio of λ = 2.5 and is dominant for λ = 3.0. However, for those highly loaded (ν = 0.25) this behaviour takes effect for λ = 3 and becomes dominant after λ = 3.5. The slenderness ratio describing a purely flexural behaviour (introduced as the (Length/width)), omitting the effect of the reduced normal force ν is not realistic. A limit of this factor taking into account the effect of the position of the shear wall (light or heavy load case of ν) is proposed $\lambda_{min} \geq 3.5 \times (1-(0.25-\nu))$. We conclude that the slenderness of λ = 3.5 is a threshold beyond which the RCW exhibits a purely flexural behaviour. Finally, it was found that Reinforced Concrete Shear Walls (RCW) capacities are very sensitive to the concrete compressive strength fc_{28}, the reduced axial load ν, the longitudinal reinforcement ratio ρ_l, the Plastic Length Lp; while being less sensitive to transverse the reinforcement ratio ρ_{sh} and the confinement zone depth CS.

However, the geometric slenderness λ is the most decisive factor affecting the NL wall response. The purpose of this study, is to go towards a future study where the RCW is studied in the context of a whole building taking into account the percentage of short and slender walls composing it, in order to propose a global factor behavior function of the ductility, λ(ν), the existing percentage of squat and slender walls.

7. Declarations

7.1. Author Contributions

Conceptualization, A.A., B.Z. and D.N.; writing—original draft preparation. A.A, B.Z. and D.N.; writing—review and editing, A.A., B.Z. and D.N. All authors have read and agreed to the published version of the manuscript.

7.2. Data Availability Statement

The data presented in this study are available in article.

7.3. Funding

The authors received no financial support for the research, authorship, and/or publication of this article.

7.4. Conflicts of Interest

The authors declare no conflict of interest.

8. References

[1] Davidovici V. "Séisme de Boumerdes. Rapport de mission". Dynamique Concept (2003). Algerian Ministry of Habitat, Urbanism and City. Available online: https://mhuv.gov.dz (accessed on May 2021).

[2] Wallace, John W., Leonardo M. Massone, Patricio Bonelli, Jeff Dragovich, René Lagos, Carl Lüders, and Jack Moehle. "Damage and Implications for Seismic Design of RC Structural Wall Buildings." In Earthquake Spectra, Vol. 28, (2012). doi:10.1193/1.4000047.

[3] Abdullah, Saman Ali. "Reinforced Concrete Structural Walls: Test Database and Modeling Parameters," PhD Dissertation University of California Los Angeles UCLA-RC Walls, (2019).

[4] Powel, G. "CSI's "Perform Components and Elements Building," (2006).

[5] European Standard. "Eurocode 8: Design of Structures for Earthquake Resistance — Part 1: General Rules, Seismic Actions and Rules for Buildings." European Committee for Standardization, (2003).

[6] ASCE 41-17 "Seismic Evaluation and Retrofit of Existing Buildings." Seismic Evaluation and Retrofit of Existing Buildings. Reston, Virginia: American Society of Civil Engineers, (2017). doi:10.1061/9780784414859.

[7] Wu, Yun Tian, Tian Qing Lan, Yan Xiao, and Yeong Bin Yang. "Macro-Modeling of Reinforced Concrete Structural Walls: State-of-the-Art." Journal of Earthquake Engineering 21, no. 4 (2017): 652–78. doi:10.1080/13632469.2016.1174754.

[8] Du, Ke, Huan Luo, Jiulin Bai, and Jingjiang Sun. "Integrating of Nonlinear Shear Models into Fiber Element for Modeling Seismic Behavior of Reinforced Concrete Coupling Beams, Wall Piers, and Overall Coupled Wall Systems." International Journal of Concrete Structures and Materials 13, no. 1 (2019): 13–34. doi:10.1186/s40069-019-0346-z.

[9] Kolozvari, Kristijan, Kamiar Kalbasi, Kutay Orakcal, Leonardo M. Massone, and John Wallace. "Shear–Flexure-Interaction Models for Planar and Flanged Reinforced Concrete Walls." Bulletin of Earthquake Engineering 17, no. 12 (2019): 6391–6417. doi:10.1007/s10518-019-00658-5.

[10] Kolozvari, Kristijan, Kamiar Kalbasi, Kutay Orakcal, and John Wallace. "Three-Dimensional Model for Nonlinear Analysis of Slender Flanged Reinforced Concrete Walls." Engineering Structures 236 (2021): 236 112105. doi:10.1016/j.engstruct.2021.112105.

[11] Mortazavi, Seyed Mohammad Reza, and Behrouz Zaeimdar. "Shear Wall Modeling with Asymmetric Openings by Macro Elements." Structures 29 (2021): 899–910. doi:10.1016/j.istruc.2020.08.049.

[12] Zhang, Zi Yu, Ran Ding, Jian Sheng Fan, Mu Xuan Tao, and Xin Nie. "Numerical Study of Reinforced Concrete Coupled Shear Walls Based on a Two-Dimensional Finite Element Model." Engineering Structures 244 (2021): 112792. doi:10.1016/j.engstruct.2021.112792.

[13] Kolozvari, Kristijan, Lauren Biscombe, Farhad Dashti, Rajesh P. Dhakal, Aysegul Gogus, M. Fethi Gullu, Richard S. Henry, et al. "State-of-the-Art in Nonlinear Finite Element Modeling of Isolated Planar Reinforced Concrete Walls." Engineering Structures 194 (2019): 46–65. doi:10.1016/j.engstruct.2019.04.097.

[14] Ugalde, David, Pablo F. Parra, and Diego Lopez-Garcia. "Assessment of the Seismic Capacity of Tall Wall Buildings Using Nonlinear Finite Element Modeling." Bulletin of Earthquake Engineering 17, no. 12 (2019): 6565–89. doi:10.1007/s10518-019-00644-x.

[15] Petrone, Floriana, Frank McKenna, Thanh Do, and David McCallen. "A Versatile Numerical Model for the Nonlinear Analysis of Squat-to-Tall Reinforced-Concrete Shear Walls." Engineering Structures 242, no. 112406 (2021). doi:10.1016/j.engstruct.2021.112406.

[16] Hellesland, J., and A. Scordelis. Analysis of RC Bridge Columns under Imposed Deforma¬tions. Delft, Netherlands: IABSE Colloquium, Delft, Netherlands, (1981): 545-559.

[17] Aktan, A. E., and V. Bertero. "Seismic Response of R/C Frame-Wall Structures"." Journal of Structural Engineering, ASCE 110, no. 8 (1984): 1803–1821.

[18] Spacone, Enrico, Filip C. Filippou, and Fabio F. Taucer. "Fibre Beam-Column Model for Non-Linear Analysis of R/C Frames: Part I. Formulation." Earthquake Engineering and Structural Dynamics 25, no. 7 (1996): 711–25. doi:10.1002/(SICI)1096-9845(199607)25:7<711::AID-EQE576>3.0.CO;2-9.

[19] Neuenhofer, Ansgar, and Filip C. Filippou. "Evaluation of Nonlinear Frame Finite-Element Models." Journal of Structural Engineering 123, no. 7 (1997): 958–66. doi:10.1061/(asce)0733-9445(1997)123:7(958).

[20] Pugh, Joshua S., Laura N. Lowes, and Dawn E. Lehman. "Nonlinear Line-Element Modeling of Flexural Reinforced Concrete Walls." Engineering Structures 104 (2015): 174–92. doi:10.1016/j.engstruct.2015.08.037.

[21] Kolozvari, Kristijan, Carlos Arteta, Matej Fischinger, Sofia Gavridou, Matias Hube, Tatjana Isaković, Laura Lowes, Kutay Orakcal, Jorge Vásquez, and John Wallace. "Comparative Study of State-of-the-Art Macroscopic Models for Planar Reinforced Concrete Walls." ACI Structural Journal 115, no. 6 (November 2018). doi:10.14359/51710835..

[22] Pozo, Juan D., Matias A. Hube, and Yahya C. Kurama. "Quantitative Assessment of Nonlinear Macro-Models for Global Behavior and Design of Planar RC Walls." Engineering Structures 224, no. 224 (2020). doi:10.1016/j.engstruct.2020.111190.

[23] Powell, Graham Harcourt. Detailed Example of a Tall Shear Wall Building: Using CSI's PERFORM 3D Nonlinear Dynamic Analysis: Nonlinear Modeling, Analysis and Performance Assessment for Earthquake Loads. Computers & Structures Incorporated, (2007).

[24] Lowes, Laura N., Dawn E. Lehman, and C. Baker. "Recommendations for modeling the nonlinear response of slender reinforced concrete walls using PERFORM-3D." In 2016 SEAOC convention. Maui, USA. (2016).

[25] Jiang, Huanjun, and Laoer Liu. "Numerical Analysis of RC Shear Walls under Cyclic Loading by PERFORM-3D." Advanced Materials Research 250–253, no. 250–253 (2011): 2253–57. doi:10.4028/www.scientific.net/AMR.250-253.2253.

[26] Wallace, J. W. "Lightly reinforced wall segments." In New Information on the Seismic Performance of Existing Concrete Buildings Seminar Notes. Oakland, CA: Earthquake Engineering Research Institute, (2006): 1-62. Available online: https://apps.peer.berkeley.edu/research/pdf/Wallace-Wall_Segments_FINAL_V3_Present.pdf (accessed on April 2021).

[27] Lowes, L. N., D. E. Lehman, and A. C. Birely. "DA Kuchma, CR Hart, KP Marley (University of Illinois, Urbana-Champaign), Behavior, Analysis, and Design of Complex Wall Systems: Planar Wall Test Program Summary Document." (2012).

[28] Kappos, Andreas. Earthquake Resistant Concrete Structures. Earthquake Resistant Concrete Structures. Taylor and Francis, 2014. doi:10.1201/9781482271300.

[29] RPA 99/Version 2003. "Algerian Seismic Regulations", Ministry of Housing Planning and the city (Ministère de l'habitat, de l'urbanisme et de la ville), Edition CGS, Algeria (2003).

[30] Paulay, T., and M. J.N. Priestley. "Stability of Ductile Structural Walls." ACI Structural Journal 90, no. 4 (1993): 385–92. doi:10.14359/3958.

[31] Park, R. "Evaluation of Ductility of Structures and Structural Assemblages from Laboratory Testing." Bulletin of the New Zealand Society for Earthquake Engineering 22, no. 3 (1989): 155–66. doi:10.5459/bnzsee.22.3.155-166.

[32] Barrera, A.C., J.L. Bonet, M.L. Romero, and M.A. Fernández. "Ductility of Slender Reinforced Concrete Columns under Monotonic Flexure and Constant Axial Load." Engineering Structures 40 (July 2012): 398–412. doi:10.1016/j.engstruct.2012.03.012.

[33] Teroaka, M, and S Fuji. "Seismic Evaluation of R/C Beam-Column Joints". In Second US-Japan Workshop on Performance-Based Earthquake Methodology for Reinforced Concrete Building Structures, Sapporo Hokkaido Japan. PEER, (2000): 379–390.

[34] Epackachi, S, N Sharma, Whitaker A., and A Hortacsu. "A Cyclic Backbone Curve for Squat RC Shear Wall"." In 11th U.S National Conference on Earthquake Engineering. June 25-29, 2018. Los Angeles, California, (2018).

[35] Kazaz, İlker. "Analytical Study on Plastic Hinge Length of Structural Walls." Journal of Structural Engineering 139, no. 11 (2013): 1938–50. doi:10.1061/(asce)st.1943-541x.0000770.

[36] A., Atmani, Boudaoud Z., and Djebbar N. "Influence of the Plastic Length on the Seismic Response of RC Shear Wall Resisting Structures." In 4th ECOCEE, 17-18 June 2019. Istanbul, Turkey, (2019).

[37] Miranda, Eduardo, and Jorge Ruiz-Garca. "Evaluation of Approximate Methods to Estimate Maximum Inelastic Displacement Demands." Earthquake Engineering and Structural Dynamics 31, no. 3 (2002): 539–60. doi:10.1002/eqe.143.

[38] Iwan, Wilfred D., and Nathan C. Gates. "Estimating Earthquake Response of Simple Hysteretic Structures." Journal of the Engineering Mechanics Division 105, no. 3 (June 1979): 391–405. doi:10.1061/jmcea3.0002481.

[39] FEMA Prestandard, "commentary for the seismic rehabilitation of buildings (FEMA356)." Washington, DC: Federal Emergency Management Agency 7, no. 2 (2000).